FA4869-08-1-4076 (AOARD-08-4076)

Research Report

Fabrication of high-performance polymer bulk-heterojunction solar cells by the interfacial modifications I.

05/01/2008 ~ 04/30/2009

Name of Principal Investigator: Tzung-Fang Guo
E-mail address: guotf@mail.ncku.edu.tw
Institution: Institute of Electro-Optical Science and Engineering, National Cheng Kung University
Mailing address: No. 1 University Road, Tainan 701, Taiwan
Phone: +886-6-2757575 ext. 65284
FAX: +886-6-2747995

Co-investigators (names and institutions): Ten-Chin Wen,
Department of Chemical Engineering, National Cheng Kung University, Tainan 701, Taiwan

Report Documentation Page

Form Approved
OMB No. 0704-0188

1. REPORT DATE	2. REPORT TYPE	3. DATES COVERED
16 JUN 2009	**FInal**	**24-04-2008 to 23-05-2009**

4. TITLE AND SUBTITLE
Fabrication of High-Performance Polymer Bulk-Heterojunction Solar Cells by Interfacial Modifications

5a. CONTRACT NUMBER
FA48690814076

5b. GRANT NUMBER

5c. PROGRAM ELEMENT NUMBER

6. AUTHOR(S)
Guo Tzung-Fang

5d. PROJECT NUMBER

5e. TASK NUMBER

5f. WORK UNIT NUMBER

7. PERFORMING ORGANIZATION NAME(S) AND ADDRESS(ES)
National Cheng Kung University,No. 1 Univeristy Road,Tainan 701,Taiwan,TW,701

8. PERFORMING ORGANIZATION REPORT NUMBER
N/A

9. SPONSORING/MONITORING AGENCY NAME(S) AND ADDRESS(ES)
AOARD, UNIT 45002, APO, AP, 96337-5002

10. SPONSOR/MONITOR'S ACRONYM(S)
AOARD

11. SPONSOR/MONITOR'S REPORT NUMBER(S)
AOARD-084076

12. DISTRIBUTION/AVAILABILITY STATEMENT
Approved for public release; distribution unlimited

13. SUPPLEMENTARY NOTES

14. ABSTRACT
This research investigated three primary tasks for fabrication of high performance polymer-bulk-heterojunction solar cells: understanding the unique organic oxide/Al interfacial properties, use of SPDPA polymer as an effective junction buffer layer, and studies of the giant magneto photo-conductance effect on them.

15. SUBJECT TERMS
Organic Materials, Solar Cells, organic and Polymeric Optical Devices

16. SECURITY CLASSIFICATION OF:			17. LIMITATION OF ABSTRACT	18. NUMBER OF PAGES	19a. NAME OF RESPONSIBLE PERSON
a. REPORT	b. ABSTRACT	c. THIS PAGE			
unclassified	**unclassified**	**unclassified**	**Same as Report (SAR)**	**63**	

Contents

I. Abstract

This research investigates three primary tasks for fabrication of high performance polymer-bulk-heterojunction solar cells. i) The fundamental studies to fully understand the unique organic oxide/Al interfacial properties at the polymer/electrode junction on the enhanced PCE of polymer BHJ solar cells. ii) The fabrication of inverted, multiple-junction polymer BHJ solar cells by applying the newly synthesized sulfonated poly(diphenylamine) (SPDPA) as an effective junction buffer layer. iii) The studies of the novel and giant magneto photo-conductance effect on polymer photovoltaic cells made of intrinsically non-magnetic organic components.

II. Technical milestones

- The fundamental studies to fully understand the unique organic oxide [poly(ethylene grycol) dimethyl ether (PEGDE)]/Al interfacial properties at the polymer/electrode junction on the enhanced PCE of polymer BHJ solar cells.

I-V curves of P3HT:PCBM based polymer BHJ solar cells with configurations of ITO glass/PEDOT:PSS/P3HT:PCBM/**PEGDE(0~6nm)**/Al(100nm) and ITO glass/PEDOT:PSS/P3HT:PCBM/PEGDE(4.5nm)/**Al(0~10nm)**/Ag(100 nm) under 1.5G illumination are presented in the following figures. The device performance was also summarized in Tables. It is found that the device performance of the BHJ solar cells, including the power conversion efficiency (*PCE:* η), V_{oc}, J_{sc}, and *FF*, are correlated with the thicknesses of both the PEGDE and Al used in the composite cathode structures. The results fortify the results of our previous studies (published in *Adv. Funct. Mater.* **18**, 3036 (2008)) regarding the instant formation of the organic oxide/Al complex at the polymer/metal junction during the vacuum thermal deposition of electrode, which is critical to the effective collection of charge carriers as well as the *PCE* of the solar cells.

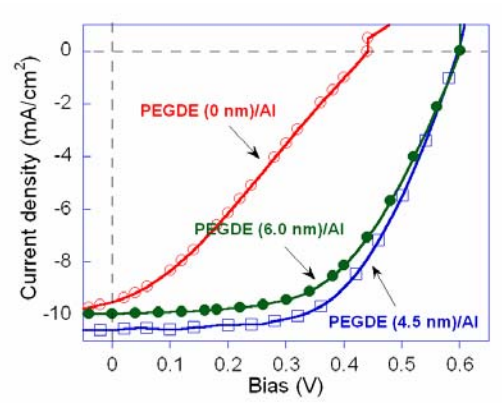

PEGDE	0 Å	45 Å	60 Å
V_{oc}	0.44	0.60	0.60
J_{sc}	9.50	10.56	9.56
V_{max}	0.22	0.40	0.40
J_{max}	5.60	8.95	8.11
FF	0.30	0.57	0.54
η(%)	1.2	3.6	3.25

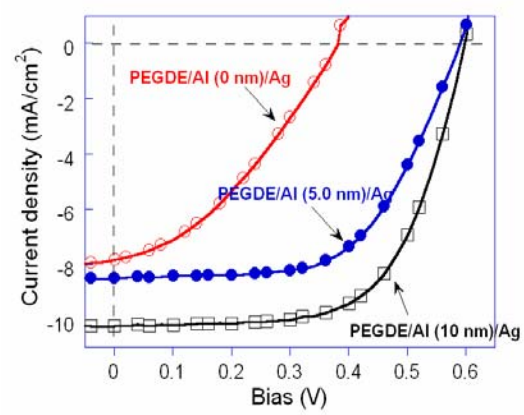

Al	0 Å	45 Å	100 Å
V_{oc}	0.38	0.58	0.60
J_{sc}	7.82	8.48	10.22
V_{max}	0.22	0.40	0.44
J_{max}	4.86	7.36	8.80
FF	0.36	0.60	0.63
η(%)	1.1	2.9	4.0

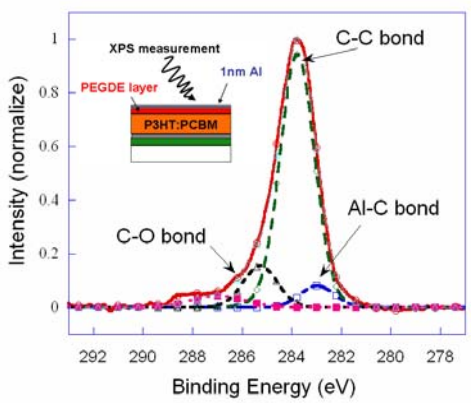

The Al-C complex is characterized by the measurement of X-ray photoelectron spectroscopy. As shown in the figure, the additional Al-C bond is observed by XPS while 3 nm of Al is deposited on the P3HT:PCBM film. The device made of the PEGDE(4.5nm)/Al(10nm)/Ag electrode has the best performance with V_{oc} of 0.60V, J_{sc} of 10.22mA/cm^2, *FF* of 0.64, and *PCE* of 4.0%. The high performance polymer BHJ solar can be fabricated without applying the low work function metals, such as Ca or Ba, as the electrodes.

- The fabrication of inverted, multiple-junction polymer BHJ solar cells by applying the newly synthesized sulfonated poly(diphenylamine) (SPDPA) as an effective junction buffer layer.

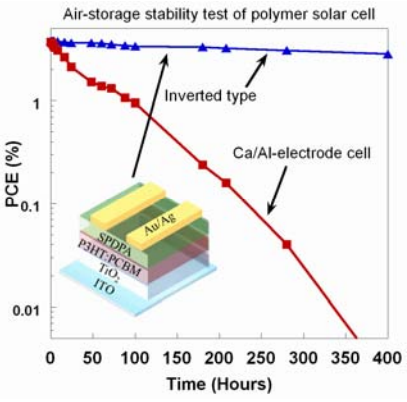

The inverted polymer solar cells of enhanced air stability were fabricated by applying titania (TiO_2) and an unique sulfonated poly(diphenylamine) (SPDPA) as the electron and hole collecting layer, respectively. The air stability of an inverted device is improved because the active layer is well encapsulated without any reactive metals. As presented in the figure, the power conversion efficiency (PCE) certainly maintained at the level above ~3.0% (~3.9% initially) after the device was stored in atmosphere without any encapsulation over than 400 hours. TiO_2 has the scavenging effect due to its photocatalytic activity and intrinsic oxygen deficiency, which may protect

the active layer from radiation damage. The conventional polymer solar cells applied Ca/Al electrode were failed immediately as soon as exposed to the air atmosphere. Our research largely improves the operation and storage lifetime of polymer BHJ solar cells.

- The studies of the novel and giant magneto photo-conductance effect on polymer photovoltaic cells made of intrinsically non-magnetic organic components.

The electrical power of polymer diodes, made of intrinsically non-magnetic components, can be extracted by a ***STEADY*** magnetic field. We presented the concept and the initial result of the novel magnetovoltaic cells that the current of a polymer diode (at zero bias or very close to zero bias without illumination) can be extracted by a steady magnetic field. As shown in the figure, while the magnetic filed is "off", the current of the diode at zero bias is at $8x10^{-7}$mA (around the detection limit of the instrument). However, as the magnetic field is "on", the current is increased to the level at $1.4x10^{-6}$ mA (a magnetovoltage can also be measured). The magnitude of magnetocurrent is found to be related to the applied magnetic field, the temperature and the blend ratio of donor/acceptor. The magneto conductance (at zero bias) versus the applied magnetic field at varied temperatures are also presented in the following figure. We disclose the magneto current is periodically varied (oscillated) with the applied magnetic field and the temperature as illustrated in the magneto conductance (at zero bias) versus the applied magnetic field plots. We attribute the novel *magnetovoltaic effect* of polymer diodes probably to the conversion of the phonon-excited energy at the charge-transfer complex states (highly related with the trap cites) in the polymer layer to the electrical power. The study here might become a novel type of the power-generation source. Although the magnetocurrent is small for a single polymer diode at current stage, the magnitude can be enhanced if multiple cells are stacked in serial or parallel. We are trying to figure out the mechanism for the generation of magnetocurrent and the oscillated magento conductance. Currently, we are working on the manuscript to submit those un-disclosed results to top journals.

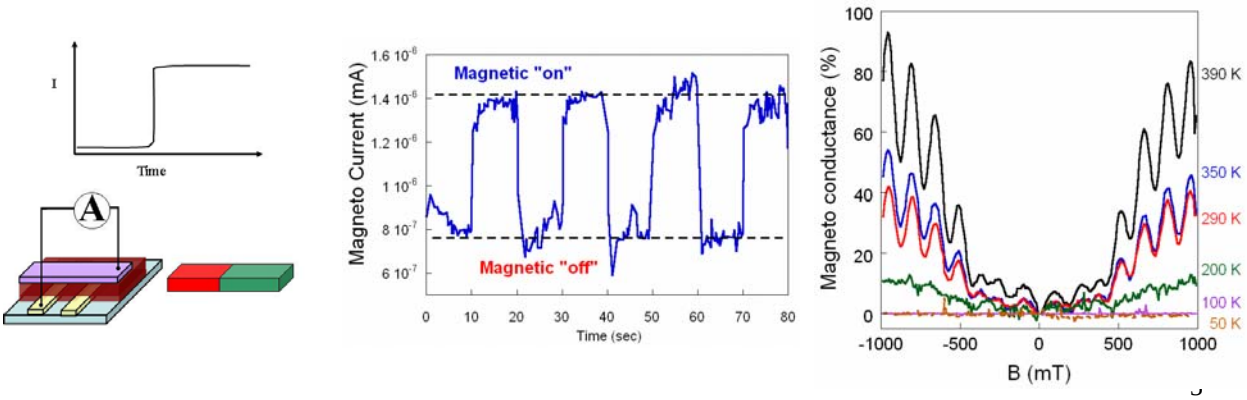

III. Summary of Accomplishments

1. "An inverted polymer photovoltaic cell with increased air stability obtained by employing novel hole/electron collecting layers" *J. Mater. Chem.* **19**, 1643 (2009). **(AOARD-08-4076)** SCI: 4.339

2. "Organic-oxide cathode buffer layer in fabricating high-performance polymer light-emitting diodes" *Adv. Funct. Mater.* **18**, 3036 (2008). **(AOARD-08-4076)** SCI: 7.496

3. "Correlation of excited states with magneto conductance response in polymer photovoltaic devices" *J. Phys. Chem. B* submitted and positively revised (2009)**. (AOARD-08-4076) (Joint research work with Prof. Bin Hu at University of Tennessee)**

4. "Nano-scale mechanical properties of polymer/fullerene bulk-heterojunction films in photovoltaic cells" manuscript will be submitted to *Appl. Phys. Lett.* soon (2009)**. (AOARD-08-4076)**

5. "Magnetovoltaic effect in polymer charge-transfer complex diodes" in preparation (2009). **(AOARD-08-4076) (Joint research work with Prof. Bin Hu at University of Tennessee)**

IV. An inverted polymer photovoltaic cell with increased air stability obtained by employing novel hole/electron collecting layers

Abstract

In this work, an inverted device was fabricated using titania (TiO_2) as the electron collecting layer (ECL) and sulfonated poly(diphenylamine) (SPDPA) as the hole collecting layer (HCL). Smooth TiO_2 film with good electron collecting ability was easily formed using the spin-coating process. The power conversion efficiency (PCE) was 3.91 %, the same as that of a conventional device. This inverted device is ascertained to maintain 2.82% PCE after 400 hours of air-storage. Because of the appropriate work functions of ECL and HCL, the interfaces at the active layer have the ohmic contacts those approach the ideal value of open circuit voltage. SPDPA helps improve the interfacial dipole effect between the active layer and the metal, as verified by *in-situ* ultraviolet photoelectron spectroscopic data.

Keywords; bulk heterojunction solar cell, inverted type, air stability, electrode buffer layer

Introduction

In the past decade, renewable energy sources such as solar cells, fuel cells, and wind energy have received increasing attention due to the depletion of fossil fuels. Among these alternative technologies, polymer bulk-heterojunction photovoltaic (PV) cells, which have a low cost and are ease to fabricate, have become an attractive research target. Devices based on poly(3-hexylthiophene) (P3HT) and fullerene derivatives, [6,6]-phenyl C_{61} butyric acid methyl ester (PCBM), have improved the conversion efficiency (PCE) to 4-5 % via the annealing process[1,2], which demonstrates that an interpenetrated network of the donor-acceptor blend can be formed for effective excition dissociation. Furthermore, devices based on low-bandgap conjugated polymers were reported to attain an average 5.5 % efficiency due to their wide absorption range[3,4]. Polymer PV cells have commercial potential because they are cost-effective.

In a conventional device, low work function metals are utilized to reduce transporting obstructions at the interface. However, these metals have a high reactivity into the oxidized state[5]. Consequently, these devices have poor life-times due to oxidation/degradation of these metals when exposed to air. A highly efficient inverted device needs to avoid any highly reactive materials. The PCE of inverted PV cells depends on effective excition dissociation and fluent carrier transporting into the collecting electrode. Thus, it is important to find the appropriate energy level of the collecting electrode to match the active layer. ITO is unsuitable as an electron collecting electrode due to the large barrier height between it and active layer. To overcome the barrier height, some researches proposed electron collecting layers (ECL), such as titanium oxide (TiO_x)[6,7] or zinc oxide (ZnO)[8], that took advantage of suitable lowest unoppied molecular orbital (LUMO) position and high environmental stability. Recently, PCE of around 4% for inverted PV cells was reported using cesium carbonate (Cs_2CO_3) as ECL and vanadium oxide (V_2O_5) as the hole collecting layer (HCL)[9]. However, the easy deliquesce of Cs_2CO_3 may be unfavorable for long-term storage and work. High work function metals such as gold (Au) and silver (Ag) usually act as hole collecting electrodes in PV cells. Unfortunately, there is still a surplus barrier height originating from the dipole effect (vacuum level alignment) between a metal and organic semiconductor film, which obstructs carrier transporting through the interface[10,11]. The dipole effect can be mitigated by inserting a heavily doped material at this interface, such as poly(3,4-ethylenedioxythiophene): poly(styrene sulfonate) (PEDOT:PSS). The challenge of using PEDOT:PSS as HCL in an inverted device is that PEDOT:PSS is an aqueous dispersion and it is difficult to coat it onto organic active layer due to its hydrophobic property. Co-solvent[6] and adhesive[9] methods were used to improve

interfacial compatibility of PEDOT:PSS. However, the conformation of PEDOT:PSS using these methods was different and consequently its work function and conductivity were changed. The change would affect the application of PEDOT:PSS to the electronic devices.

In this work, we employ an HCL, sulfonated poly(diphenylamine) (SPDPA) with environmental stability[13], and an ECL, titania (TiO_2), to construct inverted PV cells. The single component and a good solubility in polar solvent of SPDPA lead to no variation of film properties. TiO_2 film with good electron collecting ability is easily fabricated by spin-coating the precursor pretitanium (IV) isopropoxide ($Ti(OC_3H_7)_4$). A device produced with our proposed HCL and ECL is expected to be air-stable. The inverted PV cell without sealing maintained a PCE of about 2.82% after 400 hours of storage testing in air (the initial PCE was about 3.81%).

Experimental Section

The TiO2 film, used as the ECL, was prepared using a facile sol-gel procedure. $Ti(OC_3H_7)_4$ (Aldrich, 99.999%), used as a precursor, was directly spin-coated onto an ITO substrate (received from RITEK Corp., 15 Ω/□) without any further treatment. Before coating $Ti(OC_3H_7)_4$, ITO was cleaned by an ultrasonic treatment in detergent, deionized water, acetone, and isopropyl alcohol sequentially. Then, ITO was treated in a UV/O_3 photoreactor to eliminate contaminants on the surface and to avoid side reactions. The spin-coating process was conducted in a nitrogen-filled glove box. The two-step coating procedure (step 1. 1000 rpm for 5 sec and step 2. 4500 rpm for 60 sec) formed a dense film on the ITO substrate. $Ti(OC_3H_7)_4$ then underwent hydrolysis and was converted into TiO_x in air for at least 1 hour. The TiO_x film underwent thermally annealing at 450 for half an hour to transform into TiO_2. The film thickness was measured to be 80 nm using a Tencor Alpha-Step 500 Surface profiler. The novel hole injection/collecting layer, SPDPA was applied in polymer light emitting diodes[13] and PV cells[14]. Details of the preparation procedure and characterization can be found in a previous work[13].

P3HT with 2 wt% (purchased from Rieke metal) and PCBM with 2 wt% (purchased from Nano-c) were mixed in 1,2-dichlorobenzene. The blend was stirred for 24 hours at room temperature in a glove box. The active layer was spin-coated at 600 rpm for 60 sec and then slowly dried in a covered glass Petri dish. The active film thickness was about 200 nm ±10 nm. SPDPA was dissolved in ethanol with 1 wt%. 10 nm of SPDPA was spin-coated onto the active layer as the top-contact hole collecting layer. The hole

collecting electrodes, consisting of Au (30 nm)/Ag (100 nm) or only Ag (100 nm), were applied by vacuum evaporation at a pressure of ~10^{-6} torr. The active area of the device was 0.08 cm^2. The conventional PV cells were also fabricated for comparative purpose. In this case, the commercial PEDOT:PSS (Baytron-P AI 4083) was used as the HCL. The current density-voltage (*J-V)* characteristics of the devices were measured with a Keithley 2400 source-measure unit using an Oriel 91160A 300W Solar Simulator (AM 1.5 G 100 $mWcm^{-2}$ irradiation) in a nitrogen-filled glove box. The illumination intensity was calibrated using a standard Si photodiode detector with a KG-5 color filter (Hamamastsu, S1133)[15]. The devices were exposed in air without sealing in the storage test. They were illuminated by the Solar Simulator in a glove box to ensure the accurate light source intensity.

Atomic force microscopy (AFM) was performed using a NanoScope Ⅲa (Digital Instruments Inc.) for observation of TiO_2 surface topography. The characteristics of TiO_2 were studied using X-ray photoelectron spectroscopy (XPS) measurements with a VG CLAM4 surface analysis system, equipped with Al Kα radiation (1486.6 eV) at the National Synchrotron Radiation Research Center, Taiwan. The XPS measurement was conducted operated below 8×10^{-10} Torr base pressure with an energy step of 0.025 eV. The interfacial properties of the polymer/metal contact were studied using ultraviolet photoelectron spectroscopy (UPS). They were also using a VG CLAM4 surface analysis system equipped with a non-monochromatic He(I) UV source (21.2 eV). In order to protect the polymeric films from contamination, all observations were made using the *in-situ* method. The Au capping layers were deposited on identical P3HT:PCBM or P3HT:PCBM/SPDPA film by an EFM3 (Omicron) electron beam deposition system in an ultra-high vacuum preparation chamber (P~8×10^{-10} Torr) connected with a UPS analysis chamber. The Au deposition rate was around 0.1Å/s as calibrated by a quartz monitor. The work functions (Φ) of the films were defined by $\Phi = h\nu - \triangle E$, where $h\nu$ is the photon energy (21.2 eV) and $\triangle E$ is determined from the distance of the binding energy between the secondary electron emission cutoff edge and HOMO edge. The absorption spectrum was analyzed using a UV-visible spectrometer from GBC Scientific Equipment, Australia (model GBC Cintra 10e). The bandgap of TiO_2 film was calculated according to $\lambda = 1240/E_g$.

Results and discussion

In this study, TiO_2 film on ITO, prepared using a facile sol-gel procedure, was employed as the ECL. An adequate work function of ECL is important to prevent the appearance of a Schottky contact between the active layer and the collecting electrode,

which reduces the open circuit voltage (V_{oc}). The UPS spectrum of our prepared TiO_2 film is shown in Fig. 1(a). The inset shows the secondary cutoff region for determining its work function (close to the molecular energy level of the conduction band for N-type semiconductors). The conduction band of TiO_2 is located at 3.9 eV, which improves the work function of ITO as an electron collecting electrode. Fig. 1 (b) shows the UV-vis spectrum of TiO_2 film. The onset of the absorption spectrum of the TiO_2 film appears at about 390 nm (3.2 eV), which matches the intrinsic bandgap of the anatase phase. The valance band was calculated to be about 7.1 eV. It is important to have a smooth ECL because a rough ITO surface frequently causes PV cell defects, such as pinholes, that lead to current leakage. The inset shows the morphology of the TiO_2 film coated on ITO as obtained using atomic force microscopy (AFM). TiO_2 has a homogeneous and smooth surface observed due to low root mean square roughness (rms~0.97 nm) compared to a bare ITO surface (rms~2.66 nm). The characteristics of this TiO_2 layer were investigated. The conversion of $Ti(OC_3H_7)_4$ into TiO_2 was also analyzed using XPS spectra. The examination method of conversion ratio was used as the previous report[16]. Based on the ratio of the O(1S) (Ti-O-Ti) peak at 530.4 eV and the O(1S) (Ti-O-X, X=C,H) contribution at 531.9 eV, the conversion of this film was estimated to be 83.4%.

From the UPS spectra, there is no interfacial barrier height between TiO_2 and PCBM (LUMO=4.3 eV). Inverted PV cells were fabricated and compared with conventional devices. Fig. 2 shows the *J-V* curves of a conventional device with an ITO/PEDOT:PSS/P3HT:PCBM/Ca/Al structure and the inverted devices. The inverted devices with/without TiO_2 as ECL were fabricated with following the structure: ITO/TiO_2/P3HT:PCBM/SPDPA/Au/Ag. SPDPA has been confirmed to be a good HCL[14]. The conventional device shows standard performance with J_{sc}=9.43 mA/cm^2, V_{oc}=0.60 V, PCE=3.74%, and fill factor (FF) =0.66. The inverted device without TiO_2 shows bad performance with J_{sc}=0.74 mA/cm^2, V_{oc}=0.08 V, FF=0.25, and PCE=0.02%, originating from pinholes due to a rough ITO surface and the incompatible energy levels between ITO and PCBM. The inverted device with the modification TiO_2 shows great performance with J_{sc}=10.46 mA/cm^2, V_{oc} =0.58 V, FF=0.64, and PCE=3.91%. It had the same V_{oc} as the conventional device, suggesting the presence of an ohmic contact between the active layer and the collecting electrode[17]. This is explained by the energy levels, as shown in the inset. The inverted device modified by TiO_x film without thermal annealing need to be exposed to UV irradiation for several minutes to demonstrate the enhanced device performance. Similar lag effects were reported in previous studies[7,18], where they were attributed to the low electron mobility of TiO_x. After thermal annealing, this lag can be diminished due to the improvement of electron mobility of the TiO_2.

As shown in Fig. 3, the inverted devices with/without SPDPA and deposited with various metals as contacts were fabricated to clarify the role of SPDPA. After introducing SPDPA, V_{oc} of the device based on Au/Ag increased from 0.22 V to 0.58 V. With pure Ag, the device showed a similar improvement (V_{oc} changed from 0.12 V to 0.56 V). The V_{oc} magnitude is the same as the difference of molecular energy between HOMO of the donor and LUMO of the acceptor when both interfaces form an ohmic contact. The device without SPDPA had an inadequate V_{oc} magnitude, which can be attributed to the barrier height between Au and P3HT. Thus, the barrier height between the hole collecting electrode and the active layer is reduced by introducing SPDPA. The decrease in the interfacial barrier height leads to improved J_{sc} and FF. The device with SPDPA based on pure Ag (PCE=3.44%) is inferior to that based on Au/Ag (PCE=3.91%) because this interface still has some barrier height (the work functions of SPDPA and Ag are 5.25 eV and 4.6 eV, respectively). Therefore, SPDPA/Au as the hole collecting electrode is a good choice. According to the above outcomes of V_{oc}, there are two kinds of contact between organic film and the metal. One is the ohmic contact in the interface between P3HT:PCBM/SPDPA and Au. The other is the Sckottky contact in the interface between P3HT:PCBM and Au. The latter is not expected from the view of the energy level position. It can be explained by the interfacial dipole barrier which aligns the vacuum level position. The interfacial dipole barrier results from charge transfer, the pillow effect, or chemical interaction[10-12].

The photoemission studies of interfaces between Au and organic film were carried out to observe the energy level alignment. Fig. 4(a) and (b) show the UPS spectra of P3HT:PCBM and P3HT:PCBM/SPDPA with various thicknesses of Au. A higher binding energy of the secondary cutoff edge indicates a lower work function. (ionization potential) In the case of P3HT:PCBM, the cutoff edge progressively shifted toward a high binding energy position after 4Å of Au was deposited, which indicates that the HOMO of P3HT:PCBM decreased to 0.3 eV. When Au was deposited onto P3HT:PCBM, the energy levels were bent by the charge redistribution due to charge transfer at the interface that achieved electrical equilibrium by aligning Fermi levels of both P3HT:PCBM and inert Au[11]. This leads to a built-in potential within several diffusion layers. Eventually, an excess interfacial dipole barrier is created between P3HT:PCBM and Au, limiting V_{oc} and device performance. When thicker Au was deposited onto P3HT:PCBM, the UPS spectra progressively showed bulk Au behavior (shifting toward low binding energy). The UPS spectra of P3HT:PCBM/SPDPA films showed different characteristics. The work function without Au deposition was calculated to be 5.25 eV, which is attributed to the work function of the SPDPA feature[13]. Before 4Å of Au was deposited, the work function of

SPDPA maintained the same energy level, indicating no interfacial dipole effect. The heavily doped amino groups in SPDPA by its own sulfonic acid should theoretically shift the Fermi level of SPDPA close to that of Au and give SPDPA metallic behaviour, resulting in ohmic contact between SPDPA and Au. Our UPS data might have a weakness around the interface between P3HT:PCBM and SPDPA. However, V_{oc} data showed that the barrier height was reduced. Several reports[19,20] corroborated our presumption. SPDPA effectively facilitates hole transport/collection between P3HT:PCBM and Au. Thus, the inverted PV cells with SPDPA had the superior performance.

TiO_2 and SPDPA were chosen for ECL and HCL, respectively, because they are air-stable. The air stability of an inverted device is expected to be improved because the active layer is well encapsulated without any reactive metals. Fig. 5 shows the decays of the device parameters, including J_{sc}, V_{oc}, FF, and PCE from the storage test without any package. Initially, the inverted device had superior performance with J_{sc}=10.26 mA/cm^2, V_{oc} =0.6 V, FF =0.63, and PCE=3.81%. After 400 hours of air-storage, the inverted device still had a high PCE of 2.82%. J_{sc} and V_{oc} just slightly decayed (J_{sc} from 10.26 mA/cm^2 to 9.34 mA/cm^2; V_{oc} from 0.6 V to 0.57 V). It is supposed that hole and electron collecting electrodes provide suitable contact for maintaining V_{oc}. The PCE decay mainly originated from the drop of FF value, which is related to the efficiency of excition dissociation and carrier transporting ability. Thus, the decay is considered to be a degradation of the active layer on the charge transporting property due to the penetration of oxygen/water into the active layer[21]. Nevertheless, the TiO_2 and SPDPA layers sandwich the active layer to moderate oxygen/water penetration. In addition, TiO_2 has the scavenging effect due to its photocatalytic activity and intrinsic oxygen deficiency[22-24] and it has strong absorption in the ultraviolet region so it may protect the active layer from radiation damage. On the contrary, all parameters of the conventional device were inferior during air-storage test. The lifetime of a conventional device rapidly declined due to the oxidization of Ca and its poor protection of the active layer. TiO_2 and SPDPA help improve air-stability of inverted polymer PV cells.

Summary

The air stability of inverted devices was improved by employing novel HCL/ECL to maintain a PCE of 2.82% after 400 hours of air-storage. The TiO_2 layer provides an appropriate work function to form an ideal contact with the active layer and a smooth surface over ITO to avoid pinholes. The interfacial dipole effect between the metal and

organic film can be improved by modifying SPDPA, being corroborated by data of V_{oc} and UPS spectra. TiO_2 and SPDPA make polymer PV cells fit for commercial products. In addition, the UPS studies show that SPDPA may be widely applied in organic semiconductor devices such as organic thin-film transistors to improve the barrier height, especially in the interface of metal deposited on organic film.

Reference

1. W. L. Ma, C. Y. Yang, X. Gong, K. Lee and A. J. Heeger, *Adv. Funct. Mater.* **2005**, *15*, 1617.
2. G. Li, V. Shrotriya, J. S. Huang, Y. Yao, T. Moriarty, K. Emery and Y. Yang, *Nat. Mater.* **2005**, *4*, 864.
3. J. Peet, J. Y. Kim, N. E. Coates, W. L. Ma, D. Moses, A. J. Heeger and G. C. Bazan, *Nat. Mater.* **2007**, *6*, 497.
4. A. M. Ballantyne, L. Chen, J. Nelson, D. D. C. Bradley, Y. Astuti, A. Maurano, C. G. Shuttle, J. R. Durrant, M. Heeney, W. Duffy and I. McCulloch, *Adv. Mater.* **2007**, *19*, 4544.
5. M. P. de Jong, L. J. van Ijzendoom, and M. J. A. de Voigt, *Appl. Phys. Lett.* **2000**, *77*, 2255.
6. C. Waldauf, M. Morana, P. Denk, P. Schilinsky, K. Coakley, S. A. Choulis and C. J. Brabec, *Appl. Phys. Lett.* **2006**, *89*, 233517.
7. R. Steim, S. A. Choulis, P. Schilinsky and C. J. Brabec, *Appl. Phys. Lett.* **2008**, *92*, 093303.
8. M. S. White, D. C. Olson, S. E. Shaheen, N. Kopidakis and D. S. Ginley, *Appl. Phys. Lett.* **2006**, *89*, 143517.
9. H. H. Liao, L. M. Chen Z. Xu, G. Li and Y. Yang, *Appl. Phys. Lett.* **2008**, *92*, 173303.
10. J. Huang, P. F. Miller, J. S. Wilson, A. J. de Mello, J. C. de Mello and D. D. C. Bradley, *Adv. Funct. Mater.* **2005**, *15*, 290.
11. H. Ishii, K. Sugiyama, E. Ito and K. Seki, *Adv. Mater.* **1999**, *11*, 605.
12. A. Kahn, N. Koch and W. Gao, *J. Polym. Sci. B.* **2003**, *41*, 2529.
13. C. Y. Li, T. C. Wen, T. F. Guo, S. S. Hou, *Polymer* **2008**, *49*, 957.
14. C. Y. Li, T. C. Wen, T. F. Guo, *J. Mater. Chem.* **2008**, *18*, 4478.
15. V. Shrotriya, G. Li, Y. Yao, T. Moriarty, K. Emery, Y. Yang, *Adv. Funct. Mater.* **16**, 2016 (2006).
16. P. A. van Hal, M. M. Wienk, J. M. Kroon, W. J. H. Verhees, L. H. Slooff, W. J. H. van Gennip, P. Jonkheijm and R. A. J. Janssen, *Adv. Mater.* **2003**, *15*, 118.
17. V. D. Mihailetchi, P. W. M. Blom, J. C. Hummeien and M. T. Rispens, *J. Appl. Phys.* **94**, 6849 (2003).
18. J. Gilot, M. M. Wienk and R. A. J. Janssen, *Appl. Phys. Lett.* **2007**, *90*, 143512.
19. H. Peisert, M. Knupfer, F. Zhang, A. Petr, L. Dunsch, J. Fink, *Appl. Phys. Lett.* **2003**, *83*, 3930.
20. H. Peisert, A. Petr, L. Dunsch, T.Chassé, M. Knupfer, *ChemPhysChem*, **2007**, *8*, 386.

21. M. S. A. Abdou, F. P. Orifino, Y. Son, S. Holdcroft, *J. Am. Chem. Soc.* **1997**, *119*, 4518.
22. A. L. Linsebigler, G. Lu, J. T. Yates, Jr., *Chem. Rev.* **1995**, *95*, 735.
23. V. E. Henrich, P. A. Cox, *The surface Science of Metal Oxides*, Cambridge University Press, Cambridge **1994**.
24. C. Noguera, *physics and chemistry of oxide surfaces*, Cambridge University Press, Cambridge **1996**.

Figure Captions

FIG. 1. The characteristics of TiO_2 film coated on an ITO substrate (a) UPS spectrum used to determine the conduction band of the TiO_2 film. (b) UV-visible absorption spectrum of TiO_2 film. Inset figure shows the surface morphology obtained using tapping mode atomic force microscopy.

FIG. 2. The current density-voltage characteristics of conventional cells (□) and those of inverted cells with the TiO_2 modification layer (▲) and without TiO_2 (◆) under AM 1.5G (100mW/cm^2) illumination. The inset figure shows the energy levels of inverted cells in this work.

FIG. 3. The current density-voltage characteristics of inverted cells using Au (△) and Ag (○) as cathodes without SPDPA and those using Au (▲) and Ag (●) with SPDPA modified under AM 1.5G (100mW/cm^2) illumination.

FIG. 4. The normalized secondary cutoff region of UPS spectra of (a) P3HT:PCBM and (b) P3HT:PCBM/SPDPA after the deposition of various thicknesses of Au.

FIG. 5. Device parameters as a function of storage time for a conventional device (□) and an inverted device (▲): (a) power conversion efficiency (PCE), (b) open circuit voltage (V_{oc}), (c) short circuit current density (J_{sc}), and (d) fill factor (FF).

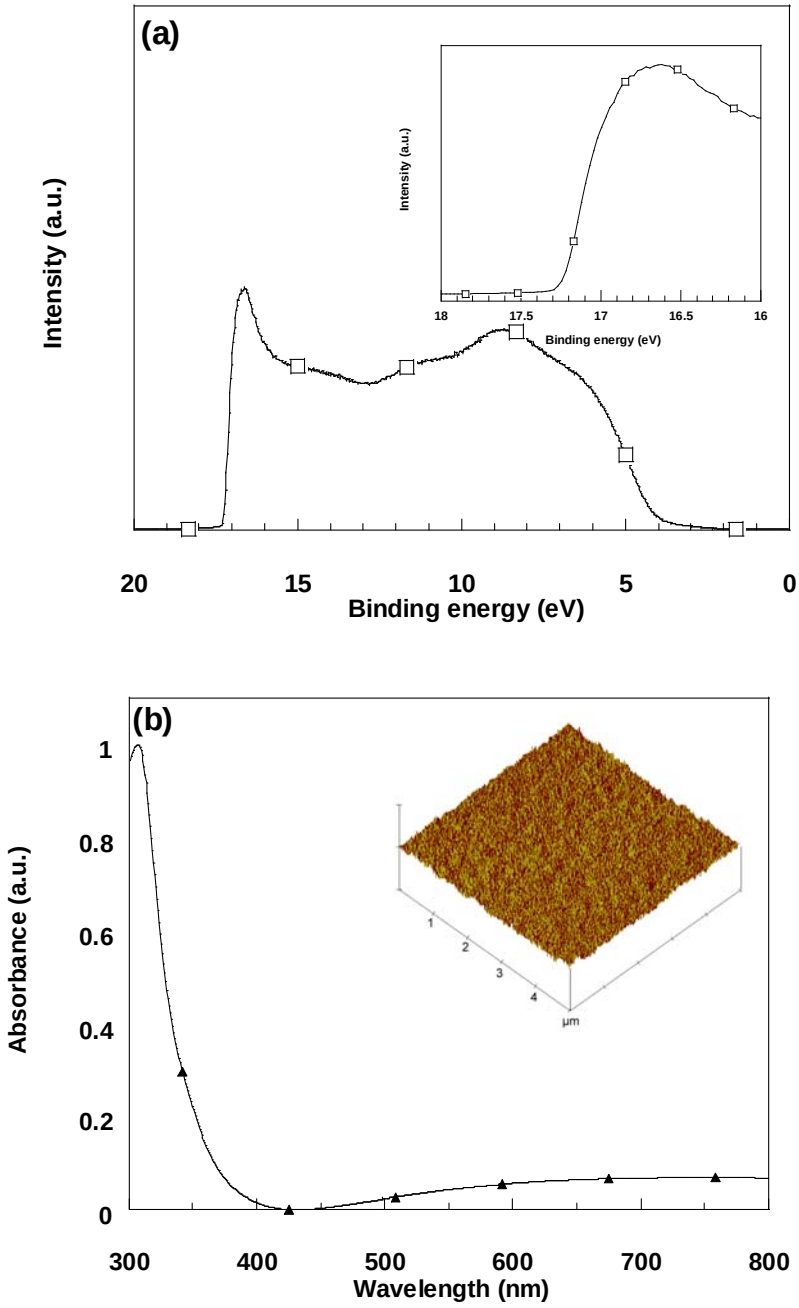
(a)
Intensity (a.u.)
Binding energy (eV)
20
15
10
5
0
Intensity (a.u.)
18
17.5
17
16.5
16
Binding energy (eV)
(b)
Absorbance (a.u.)
1
0.8
0.6
0.4
0.2
0
300
400
500
600
700
800
Wavelength (nm)
1
2
3
4
µm

Fig. 1.

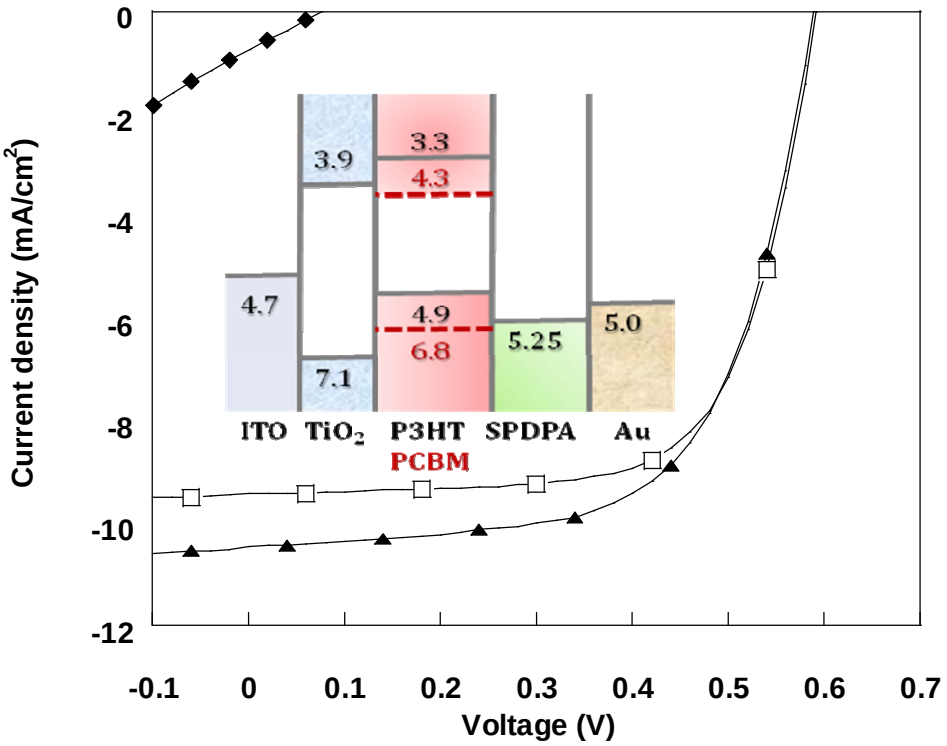
0
-2
-4
-6
-8
-10
-12
-0.1
0
0.1
0.2
0.3
0.4
0.5
0.6
0.7
Current density (mA/cm2)
Voltage (V)
3.9
3.3
4.3
4.7
4.9
6.8
5.25
5.0
7.1
ITO
TiO2
P3HT
PCBM
SPDPA
Au

Fig. 2.

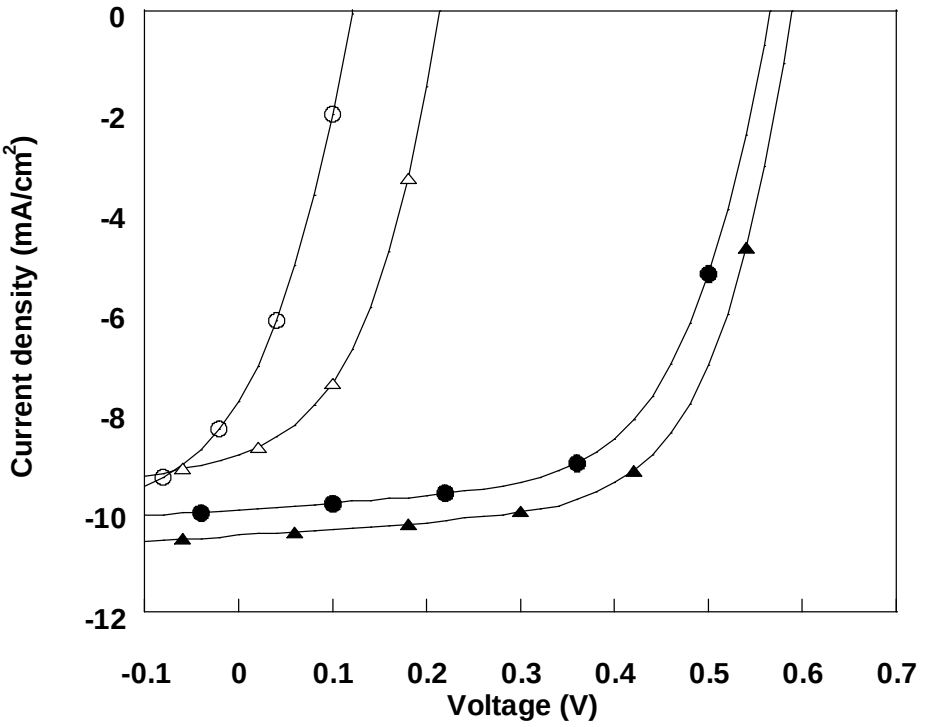
0
-2
-4
-6
-8
-10
-12
Current density (mA/cm2)
-0.1
0
0.1
0.2
0.3
0.4
0.5
0.6
0.7
Voltage (V)

Fig. 3.

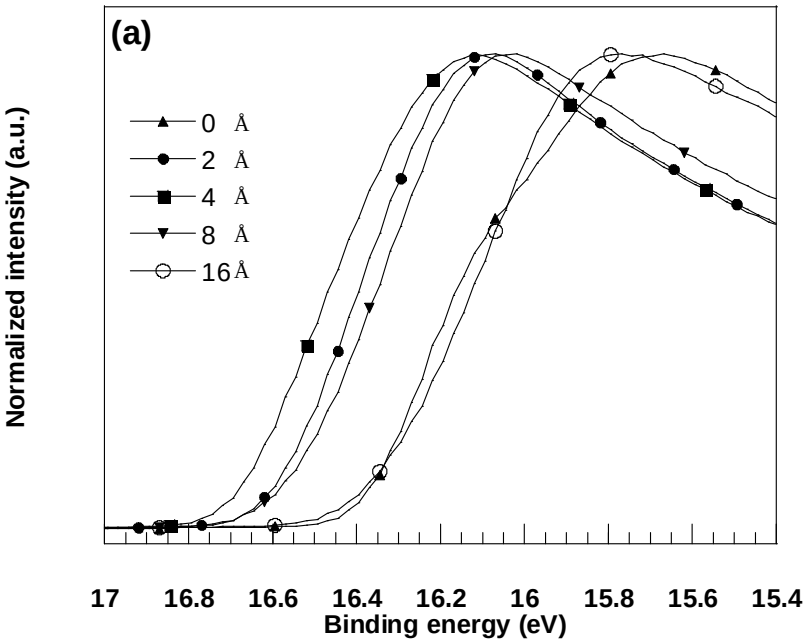
(a)
0 Å
2 Å
4 Å
8 Å
16 Å
Normalized intensity (a.u.)
17
16.8
16.6
16.4
16.2
16
15.8
15.6
15.4
Binding energy (eV)

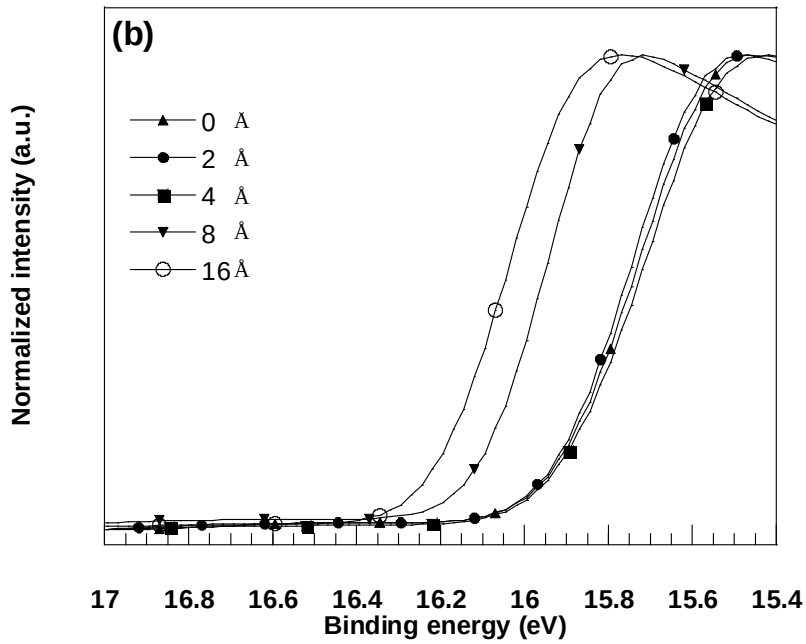
(b)
0 Å
2 Å
4 Å
8 Å
16 Å
Normalized intensity (a.u.)
17
16.8
16.6
16.4
16.2
16
15.8
15.6
15.4
Binding energy (eV)

Fig. 4.

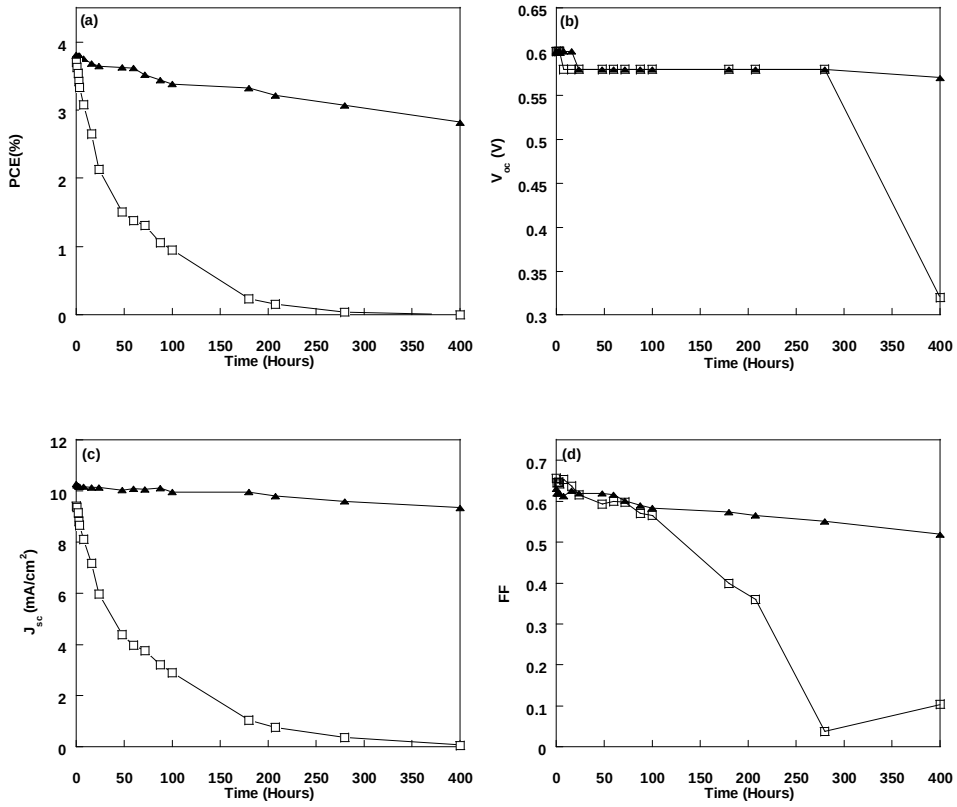
(a)
PCE(%)
Time (Hours)
(b)
V_{oc} (V)
Time (Hours)
(c)
J_{sc} (mA/cm^2)
Time (Hours)
(d)
FF
Time (Hours)

Fig. 5.

V. Future work

- Summarize and continue on the work of applying organic oxide/Al complex electrode for the high-performance BHJ solar cells. In addition, depth-profile measurement of X-ray photoelectron spectroscopy will be used to *in-situ* characterize the unique carbon-metal properties at the cathode interface, in which XPS experiment will be conduct at National Synchrotron Radiation Research Center, Taiwan. Micro Raman scattering spectroscopy, Fourier transform infrared spectroscopy, and Atomic force microscopy will also be used to characterize the unique organic oxide/Al complex layer at the polymer/metal junction in charge generation and transport processes. The performance of the organic oxide/Al electrode-based BHJ polymer solar cell devices would be well optimized.
- SPDPA-functionalized charge collecting electrodes had been successfully applied to the normal- and inverted-type polymer BHJ solar cells in our current studies. We propose to newly synthesize the SPDPA-based derivatives with the better molecular weight distribution and charge transport mobility. The performance of the inverted polymer BHJ solar cells would be optimized to enhance the air stability in the operation and storage test. Additionally, polymer BHJ solar cells of the tandem configuration would be tested. We plan to increase the *PCE* through the stacking of the multiple junction cells. The applying of the appropriate hole-collecting, electron-collecting, and the cells-collecting layers would be critical to the balance of the charge carriers and the overall *PCE*.
- A periodically oscillated magnetocurrent or magnetovoltage is generated from a polymer diode by the applied magnetic field in our studies. We suggest the mechanisms of the magnetovoltaic effect to be the conversion of the phonon-induced energy from the intermolecular charge-transfer complex at the P3HT and PCBM sites. The oscillated magneto conductance is presumable to be the quantized states (delocalized or vibrational states) of the charge-transfer complex. To understand the mechanisms for the generation of magnetocurrent and magentovoltage by varying the composition of the donor/acceptor-based polymer diode, magnitude of the applied magnetic filed and temperature, and the electrode would be the novel studies in our future work.

VI. Conclusions

Polymer BHJ solar cells applying organic oxide/Al composite electrode had been successfully demonstrated in our current studies. *PCE* of 4.0%, V_{oc} of 0.60V, J_{sc} of 10.22 mA/cm^2, and *FF* of 0.63 are presented in our work. Our recent studies also indicated the co-evaporation of PEGDE and Al at different ratio can be used as an effective electrode instead of the PEGDE/Al double layer configuration for polymer BHJ solar cells. Comprehensive analysis of the XPS measurement on the PEGDE:Al and PEGDE/Al junction had been studied. Three manuscripts and one patent regarding this subject are under the preparation, which would be submitted as soon as possible.

The inverted-type polymer solar cells of enhanced air stability were fabricated by applying titania (TiO_2) and an unique sulfonated poly(diphenylamine) (SPDPA) as the electron and hole collecting layer, respectively. [Li *et al.*, *J. Mater. Chem.* **2009**, 19, 1643] The initial power conversion efficiency (PCE) of the inverted-type polymer solar cells is ~3.9% (V_{oc}=0.58, I_{sc}=10.46mA/cm^2, *FF*=0.65) and certainly maintained at the level above ~3.0% after the devices were stored in atmosphere without any encapsulation over than 400 hours. Newly synthesize the SPDPA-based derivatives with the better molecular weight distribution and charge transport mobility would be used to increase the device performance and extend the operation lifetime.

The dissociation and the charge-reaction processes of the photo-excited states in organic semiconductor layers that transform into free charge carriers are susceptible to change by the applied magnetic filed and essentially important to MC responses in organic/polymer diodes and PV cells. The recently disclosed ″Magnetovoltaic effect″ suggests the extraction of a magnetocurrent from polymer diodes by a steady magnetic field possibly through the conversion of the phonon-excited states. This is a very important phenomenon in physics and energy related applications. Two manuscripts are prepared and will be submitted soon.

An inverted polymer photovoltaic cell with increased air stability obtained by employing novel hole/electron collecting layers

Chen-Yan Li,[a] Ten-Chin Wen,*[a] Tsung-Hsun Lee,[c] Tzung-Fang Guo,*[b] Jung-Chun-Andrew Huang,[c] Ying-Chang Lin[d] and Yao-Jane Hsu[d]

Received 5th September 2008, Accepted 9th December 2008
First published as an Advance Article on the web 3rd February 2009
DOI: 10.1039/b815523b

In this work, an inverted device was fabricated using titania (TiO_2) as the electron collecting layer (ECL) and sulfonated poly(diphenylamine) (SPDPA) as the hole collecting layer (HCL). Smooth TiO_2 film with good electron collecting ability was easily formed using the spin-coating process. The power conversion efficiency (PCE) was 3.91%, the same as that of a conventional device. This inverted device is ascertained to maintain 2.82% PCE after 400 h of air-storage. Because of the appropriate work functions of ECL and HCL, the interfaces at the active layer have the ohmic contacts those approach the ideal value of open circuit voltage. SPDPA helps improve the interfacial dipole effect between the active layer and the metal, as verified by *in-situ* ultraviolet photoelectron spectroscopic data.

Introduction

In the past decade, renewable energy sources such as solar cells, fuel cells, and wind energy have received increasing attention due to the depletion of fossil fuels. Among these alternative technologies, polymer bulk-heterojunction photovoltaic (PV) cells, which have a low cost and are easy to fabricate, have become an attractive research target. Devices based on poly(3-hexylthiophene) (P3HT) and fullerene derivatives, [6,6]-phenyl C_{61} butyric acid methyl ester (PCBM), have improved the conversion efficiency (PCE) to 4–5% *via* the annealing process,[1,2] which demonstrates that an interpenetrated network of the donor–acceptor blend can be formed for effective exciton dissociation. Furthermore, devices based on low-bandgap conjugated polymers were reported to attain an average 5.5% efficiency due to their wide absorption range.[3,4] Polymer PV cells have commercial potential because they are cost-effective.

In a conventional device, low work function metals are utilized to reduce transporting obstructions at the interface. However, these metals have a high reactivity into the oxidized state.[5] Consequently, these devices have poor life-times due to oxidation/degradation of these metals when exposed to air. A highly efficient inverted device needs to avoid any highly reactive materials. The PCE of inverted PV cells depends on effective exciton dissociation and fluent carrier transporting into the collecting electrode. Thus, it is important to find the appropriate energy level of the collecting electrode to match the active layer. ITO is unsuitable as an electron collecting electrode due to the large barrier height between it and the active layer. To overcome the barrier height, some researches proposed electron collecting layers (ECL), such as titanium oxide (TiO_x)[6,7] or zinc oxide (ZnO),[8] that took advantage of suitable lowest unoccupied molecular orbital (LUMO) positions and high environmental stability. Recently, PCE of around 4% for inverted PV cells was reported using cesium carbonate (Cs_2CO_3) as ECL and vanadium oxide (V_2O_5) as the hole collecting layer (HCL).[9] However, the easy deliquesce of Cs_2CO_3 may be unfavorable for long-term storage and work. High work function metals such as gold (Au) and silver (Ag) usually act as hole collecting electrodes in PV cells. Unfortunately, there is still a surplus barrier height originating from the dipole effect (vacuum level alignment) between a metal and organic semiconductor film, which obstructs carrier transporting through the interface.[10,11] The dipole effect can be mitigated by inserting a heavily doped material at this interface, such as poly(3,4-ethylenedioxythiophene):poly(styrene sulfonate) (PEDOT:PSS). The challenge of using PEDOT:PSS as HCL in an inverted device is that PEDOT:PSS is an aqueous dispersion and it is difficult to coat it onto an organic active layer due to its hydrophobic property. Co-solvent[6] and adhesive[9] methods were used to improve interfacial compatibility of PEDOT:PSS. However, the conformation of PEDOT:PSS using these methods was different and consequently its work function and conductivity were changed.[12] The change would affect the application of PEDOT:PSS to electronic devices.

In this work, we employ an HCL, sulfonated poly(diphenylamine) (SPDPA) with environmental stability,[13] and an ECL, titania (TiO_2), to construct inverted PV cells. The single component and a good solubility in polar solvent of SPDPA lead to no variation of film properties. TiO_2 film with good electron collecting ability is easily fabricated by spin-coating the precursor pretitanium(IV) isopropoxide ($Ti(OC_3H_7)_4$). A device produced with our proposed HCL and ECL is expected to be air-stable. The inverted PV cell without sealing maintained a PCE of about 2.82% after 400 h of storage testing in air (the initial PCE was about 3.81%).

[a]*Department of Chemical Engineering, Advanced Optoelectronic Technology Center, National Cheng Kung University, Tainan, 70101, Taiwan. E-mail: tcwen@mail.ncku.edu.tw*
[b]*Institute of Electro-Optical Science and Engineering, Advanced Optoelectronic Technology Center, National Cheng Kung University, Tainan, 70101, Taiwan. E-mail: guotf@mail.ncku.edu.tw*
[c]*Department of Physics, Advanced Optoelectronic Technology Center, National Cheng Kung University, Tainan, 70101, Taiwan*
[d]*National Synchrotron Radiation Research Center, Hsinchu, 30076, Taiwan*

Experimental

The TiO_2 film, used as the ECL, was prepared using a facile sol–gel procedure. $Ti(OC_3H_7)_4$ (Aldrich, 99.999%), used as a precursor, was directly spin-coated onto an ITO substrate (received from RITEK Corp., 15 Ω/square) without any further treatment. Before coating with $Ti(OC_3H_7)_4$, the ITO was cleaned by an ultrasonic treatment in detergent, deionized water, acetone, and isopropyl alcohol, sequentially. Then, the ITO was treated in a UV/O_3 photoreactor to eliminate contaminants on the surface and to avoid side reactions. The spin-coating process was conducted in a nitrogen-filled glove box. The two-step coating procedure (step 1. 1000 rpm for 5 s and step 2. 4500 rpm for 60 s) formed a dense film on the ITO substrate. $Ti(OC_3H_7)_4$ then underwent hydrolysis and was converted into TiO_x in air for at least 1 h. The TiO_x film underwent thermal annealing at 450 °C for half an hour to transform into TiO_2. The film thickness was measured to be 80 nm using a Tencor Alpha-Step 500 Surface profiler. The novel hole injection/collecting layer, SPDPA, was applied in polymer light emitting diodes[13] and PV cells.[14] Details of the preparation procedure and characterization can be found in a previous work.[13]

P3HT with 2 wt% (purchased from Rieke metal) and PCBM with 2 wt% (purchased from Nano-c) were mixed in 1,2-dichlorobenzene. The blend was stirred for 24 h at room temperature in a glove box. The active layer was spin-coated at 600 rpm for 60 s and then slowly dried in a covered glass Petri dish. The active film thickness was about 200 nm ±10 nm. SPDPA was dissolved in ethanol with 1 wt%. 10 nm of SPDPA was spin-coated onto the active layer as the top-contact hole collecting layer. The hole collecting electrodes, consisting of Au (30 nm)/Ag (100 nm) or only Ag (100 nm), were applied by vacuum evaporation at a pressure of $\sim 10^{-6}$ torr. The active area of the device was 0.08 cm^2. The conventional PV cells were also fabricated for comparative purpose. In this case, the commercial PEDOT:PSS (Baytron-P AI 4083) was used as the HCL. The current density-voltage (*J-V*) characteristics of the devices were measured with a Keithley 2400 source-measure unit using an Oriel 91160A 300W Solar Simulator (AM 1.5 G 100 mW cm^{-2} irradiation) in a nitrogen-filled glove box. The illumination intensity was calibrated using a standard Si photodiode detector with a KG-5 color filter (Hamamastsu, S1133).[15] The devices were exposed in air without sealing in the storage test. They were illuminated by the Solar Simulator in a glove box to ensure the accurate light source intensity.

Atomic force microscopy (AFM) was performed using a NanoScope IIIa (Digital Instruments Inc.) for observation of TiO_2 surface topography. The characteristics of TiO_2 were studied using X-ray photoelectron spectroscopy (XPS) measurements with a VG CLAM4 surface analysis system, equipped with Al Kα radiation (1486.6 eV) at the National Synchrotron Radiation Research Center, Taiwan. The XPS measurements were conducted below 8×10^{-10} Torr base pressure with an energy step of 0.025 eV. The interfacial properties of the polymer/metal contact were studied using ultraviolet photoelectron spectroscopy (UPS). They were also studied using a VG CLAM4 surface analysis system equipped with a non-monochromatic He(I) UV source (21.2 eV). In order to protect the polymeric films from contamination, all observations were made using the *in-situ* method. The Au capping layers were deposited on identical P3HT:PCBM or P3HT:PCBM/SPDPA film by an EFM3 (Omicron) electron beam deposition system in an ultra-high vacuum preparation chamber ($P \sim 8 \times 10^{-10}$ Torr) connected with a UPS analysis chamber. The Au deposition rate was around 0.1 Å/s as calibrated by a quartz monitor. The work functions (Φ) of the films were defined by $\Phi = h\nu - \triangle E$, where $h\nu$ is the photon energy (21.2 eV) and $\triangle E$ is determined from the distance of the binding energy between the secondary electron emission cutoff edge and the HOMO edge. The absorption spectrum was analyzed using a UV-visible spectrometer from GBC Scientific Equipment, Australia (model GBC Cintra 10e). The bandgap of TiO_2 film was calculated according to $\lambda = 1240/E_g$.

Results

In this study, TiO_2 film on ITO, prepared using a facile sol–gel procedure, was employed as the ECL. An adequate work function of ECL is important to prevent the appearance of a Schottky

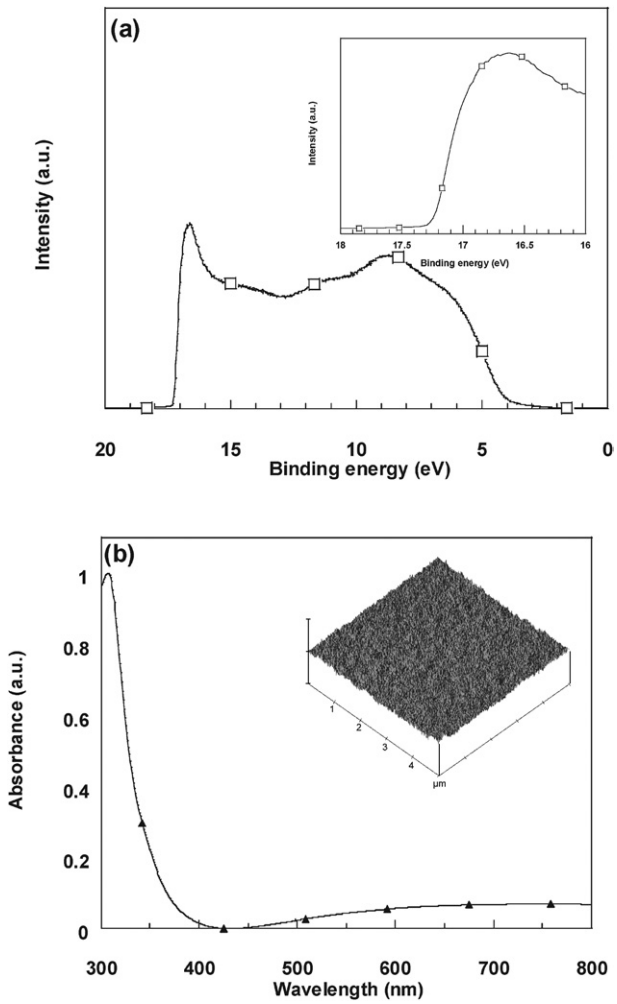

Fig. 1 The characteristics of TiO_2 film coated on an ITO substrate. (a) UPS spectrum used to determine the conduction band of the TiO_2 film. (b) UV-visible absorption spectrum of TiO_2 film. Inset figure shows the surface morphology obtained using tapping mode atomic force microscopy.

contact between the active layer and the collecting electrode, which reduces the open circuit voltage (V_{oc}). The UPS spectrum of our prepared TiO_2 film is shown in Fig. 1(a). The inset shows the secondary cutoff region for determining its work function (close to the molecular energy level of the conduction band for N-type semiconductors). The conduction band of TiO_2 is located at 3.9 eV, which improves the work function of ITO as an electron collecting electrode. Fig. 1 (b) shows the UV-vis spectrum of TiO_2 film. The onset of the absorption spectrum of the TiO_2 film appears at about 390 nm (3.2 eV), which matches the intrinsic bandgap of the anatase phase. The valance band was calculated to be about 7.1 eV. It is important to have a smooth ECL because a rough ITO surface frequently causes PV cell defects, such as pinholes, that lead to current leakage. The inset shows the morphology of the TiO_2 film coated on ITO as obtained using atomic force microscopy (AFM). TiO_2 has a homogeneous and smooth surface observed due to low root mean square roughness (rms $\sim$ 0.97 nm) compared to a bare ITO surface (rms $\sim$ 2.66 nm). The characteristics of this TiO_2 layer were investigated. The conversion of $Ti(OC_3H_7)_4$ into TiO_2 was also analyzed using XPS spectra. The examination method of the conversion ratio was used as the previous report.[16] Based on the ratio of the O(1S) (Ti–O–Ti) peak at 530.4 eV and the O(1S) (Ti–O–X, X = C,H) contribution at 531.9 eV, the conversion of this film was estimated to be 83.4%.

From the UPS spectra, there is no interfacial barrier height between TiO_2 and PCBM (LUMO = 4.3 eV). Inverted PV cells were fabricated and compared with conventional devices. Fig. 2 shows the *J-V* curves of a conventional device with an ITO/PEDOT:PSS/P3HT:PCBM/Ca/Al structure and the inverted devices. The inverted devices with/without TiO_2 as ECL were fabricated with the following structure: ITO/TiO_2/P3HT:PCBM/SPDPA/Au/Ag. SPDPA has been confirmed to be a good HCL.[13] The conventional device shows standard performance with J_{sc} = 9.43 mA/cm^2, V_{oc} = 0.60 V, PCE = 3.74%, and fill factor (FF) = 0.66. The inverted device without TiO_2 shows bad performance with J_{sc} = 0.74 mA/cm^2, V_{oc} = 0.08 V, FF = 0.25, and PCE = 0.02%, originating from pinholes due to a rough ITO surface and the incompatible energy levels between ITO and PCBM. The inverted device with the modification TiO_2 shows great performance with J_{sc} = 10.46 mA/cm^2, V_{oc} = 0.58 V, FF = 0.64, and PCE = 3.91%. It had the same V_{oc} as the conventional device, suggesting the presence of an ohmic contact between the active layer and the collecting electrode.[17] This is explained by the energy levels, as shown in the inset. The inverted device modified by TiO_x film without thermal annealing need to be exposed to UV irradiation for several minutes to demonstrate the enhanced device performance. Similar lag effects were reported in previous studies,[7,18] where they were attributed to the low electron mobility of TiO_x. After thermal annealing, this lag can be diminished due to the improvement of electron mobility of the TiO_2.

As shown in Fig. 3, the inverted devices with/without SPDPA and deposited with various metals as contacts were fabricated to clarify the role of SPDPA. After introducing SPDPA, V_{oc} of the device based on Au/Ag increased from 0.22 V to 0.58 V. With pure Ag, the device showed a similar improvement (V_{oc} changed from 0.12 V to 0.56 V). The V_{oc} magnitude is the same as the difference of molecular energy between HOMO of the donor and LUMO of the acceptor when both interfaces form an ohmic contact. The device without SPDPA had an inadequate V_{oc} magnitude, which can be attributed to the barrier height between Au and P3HT. Thus, the barrier height between the hole collecting electrode and the active layer is reduced by introducing SPDPA. The decrease in the interfacial barrier height leads to improved J_{sc} and FF. The device with SPDPA based on pure Ag (PCE = 3.44%) is inferior to that based on Au/Ag (PCE = 3.91%) because this interface still has some barrier height (the work functions of SPDPA and Ag are 5.25 eV and 4.6 eV, respectively). Therefore, SPDPA/Au as the hole collecting electrode is a good choice. According to the above outcomes of V_{oc}, there are two kinds of contact between organic film and the metal. One is the ohmic contact in the interface between P3HT:PCBM/SPDPA and Au. The other is the Sckottky contact in the interface between P3HT:PCBM and Au. The latter is not expected from

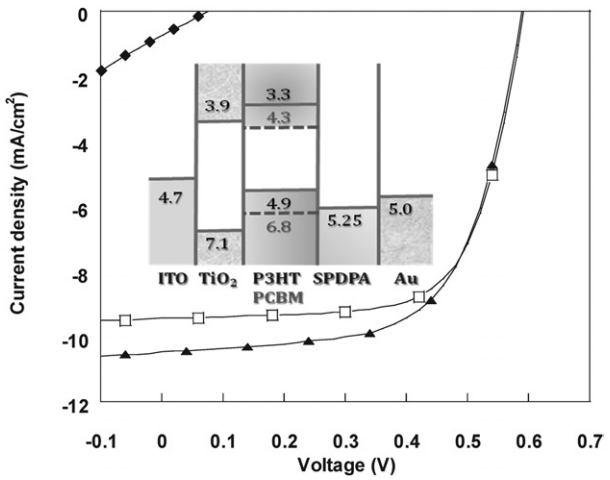

Fig. 2 The current density-voltage characteristics of conventional cells (□) and those of inverted cells with the TiO_2 modification layer (▲) and without TiO_2 (◆) under AM 1.5 G (100 mW/cm^2) illumination. The inset figure shows the energy levels of inverted cells in this work.

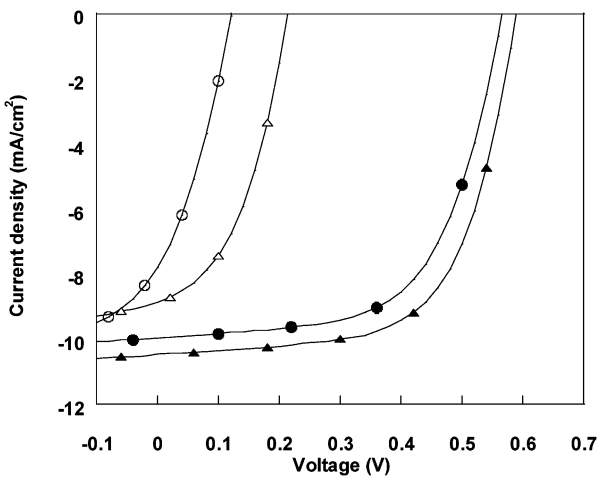

Fig. 3 The current density-voltage characteristics of inverted cells using Au (△) and Ag (○) as cathodes without SPDPA and those using Au (▲) and Ag (●) with SPDPA modified under AM 1.5 G (100 mW/cm^2) illumination.

the view of the energy level position. It can be explained by the interfacial dipole barrier which aligns with the vacuum level position. The interfacial dipole barrier results from charge transfer, the pillow effect, or chemical interaction.[10,11]

The photoemission studies of interfaces between Au and organic film were carried out to observe the energy level alignment. Fig. 4(a) and (b) show the UPS spectra of P3HT:PCBM and P3HT:PCBM/SPDPA with various thicknesses of Au. A higher binding energy of the secondary cutoff edge indicates a lower work function (ionization potential). In the case of P3HT:PCBM, the cutoff edge progressively shifted towards a high binding energy position after 4 Å of Au was deposited, which indicated that the HOMO of P3HT:PCBM decreased to 0.3 eV. When Au was deposited onto P3HT:PCBM, the energy levels were bent by the charge redistribution due to charge transfer at the interface that achieved electrical equilibrium by aligning Fermi levels of both P3HT:PCBM and inert Au.[10] This leads to a built-in potential within several diffusion layers. Eventually, an excess interfacial dipole barrier was created between P3HT:PCBM and Au, limiting V_{oc} and device performance. When thicker Au was deposited onto P3HT:PCBM, the UPS spectra progressively showed bulk Au behavior (shifting towards low binding energy). The UPS spectra of P3HT:PCBM/SPDPA films showed different characteristics. The work function without Au deposition was calculated to be 5.25 eV, which was attributed to the work function of the SPDPA feature.[12] Before 4 Å of Au was deposited, the work function of SPDPA maintained the same energy level, indicating no interfacial dipole effect. The heavily doped amino groups in SPDPA by its own sulfonic acid should theoretically shift the Fermi level of SPDPA close to that of Au and give SPDPA metallic behaviour, resulting in ohmic contact between SPDPA and Au. Our UPS data might have a weakness around the interface between P3HT:PCBM and SPDPA. However, V_{oc} data showed that the barrier height was reduced. Several reports[19,20] corroborated our presumption. SPDPA effectively facilitates hole transport/collection between P3HT:PCBM and Au. Thus, the inverted PV cells with SPDPA had the superior performance.

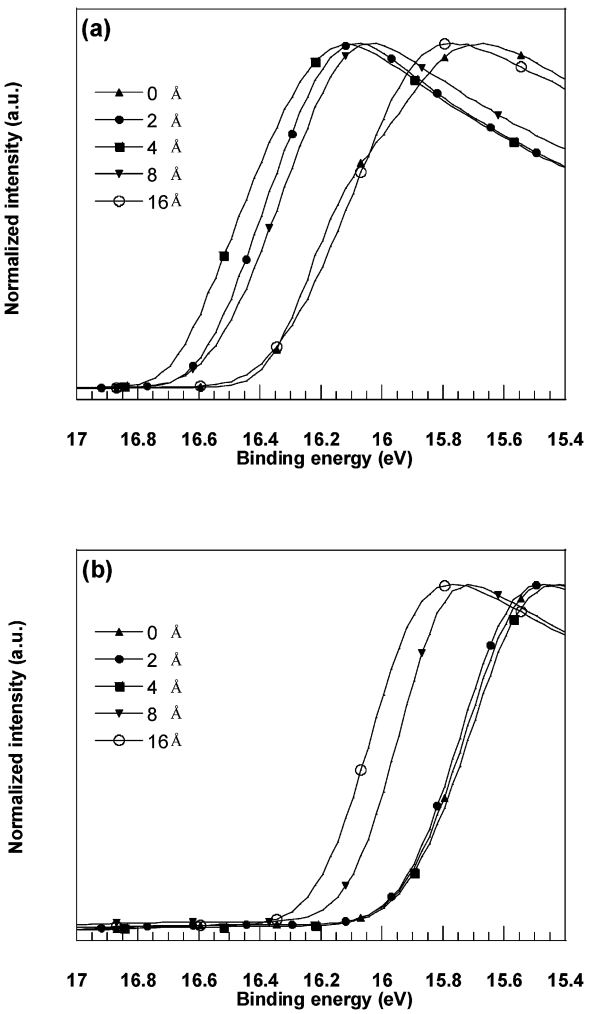

Fig. 4 The normalized secondary cutoff region of UPS spectra of (a) P3HT:PCBM and (b) P3HT:PCBM/SPDPA after the deposition of various thicknesses of Au.

TiO_2 and SPDPA were chosen for ECL and HCL, respectively, because they are air-stable. The air-stability of an inverted device is expected to be improved because the active layer is well encapsulated without any reactive metals. Fig. 5 shows the decays of the device parameters, including J_{sc}, V_{oc}, FF, and PCE from the storage test without any package. Initially, the inverted device had superior performance with $J_{sc} = 10.26$ mA/cm^2, $V_{oc} = 0.6$ V, FF = 0.63, and PCE = 3.81%. After 400 h of air-storage, the inverted device still had a high PCE of 2.82%. J_{sc} and V_{oc} just slightly decayed (J_{sc} from 10.26 mA/cm^2 to 9.34 mA/cm^2; V_{oc} from 0.6 V to 0.57 V). It is supposed that hole and electron collecting electrodes provide suitable contact for maintaining V_{oc}. The PCE decay mainly originated from the drop of FF value, which is related to the efficiency of exciton dissociation and carrier transporting ability. Thus, the decay was considered to be a degradation of the active layer on the charge transporting property due to the penetration of oxygen/water into the active layer.[21] Nevertheless, the TiO_2 and SPDPA layers sandwiched the active layer to moderate oxygen/water penetration. In addition, TiO_2 has the scavenging effect due to its photocatalytic activity and intrinsic oxygen deficiency[22–24] and it has strong absorption in the ultraviolet region so it may protect the active layer from radiation damage. On the contrary, all parameters of the conventional device were inferior during air-storage tests. The lifetime of a conventional device rapidly declined due to the oxidization of Ca and its poor protection of the active layer. TiO_2 and SPDPA help improve air-stability of inverted polymer PV cells.

Conclusion

The air-stability of inverted devices was improved by employing novel HCL/ECL to maintain a PCE of 2.82% after 400 h of air-storage. The TiO_2 layer provides an appropriate work function to form an ideal contact with the active layer and a smooth surface over ITO to avoid pinholes. The interfacial dipole effect between the metal and organic film can be improved by modifying SPDPA, being corroborated by data of V_{oc} and UPS spectra. TiO_2 and SPDPA make polymer PV cells fit for commercial products. In addition, the UPS studies show that SPDPA may be widely applied in organic semiconductor devices such as organic thin-film transistors to improve the barrier height, especially in the interface of metal deposited on organic film.

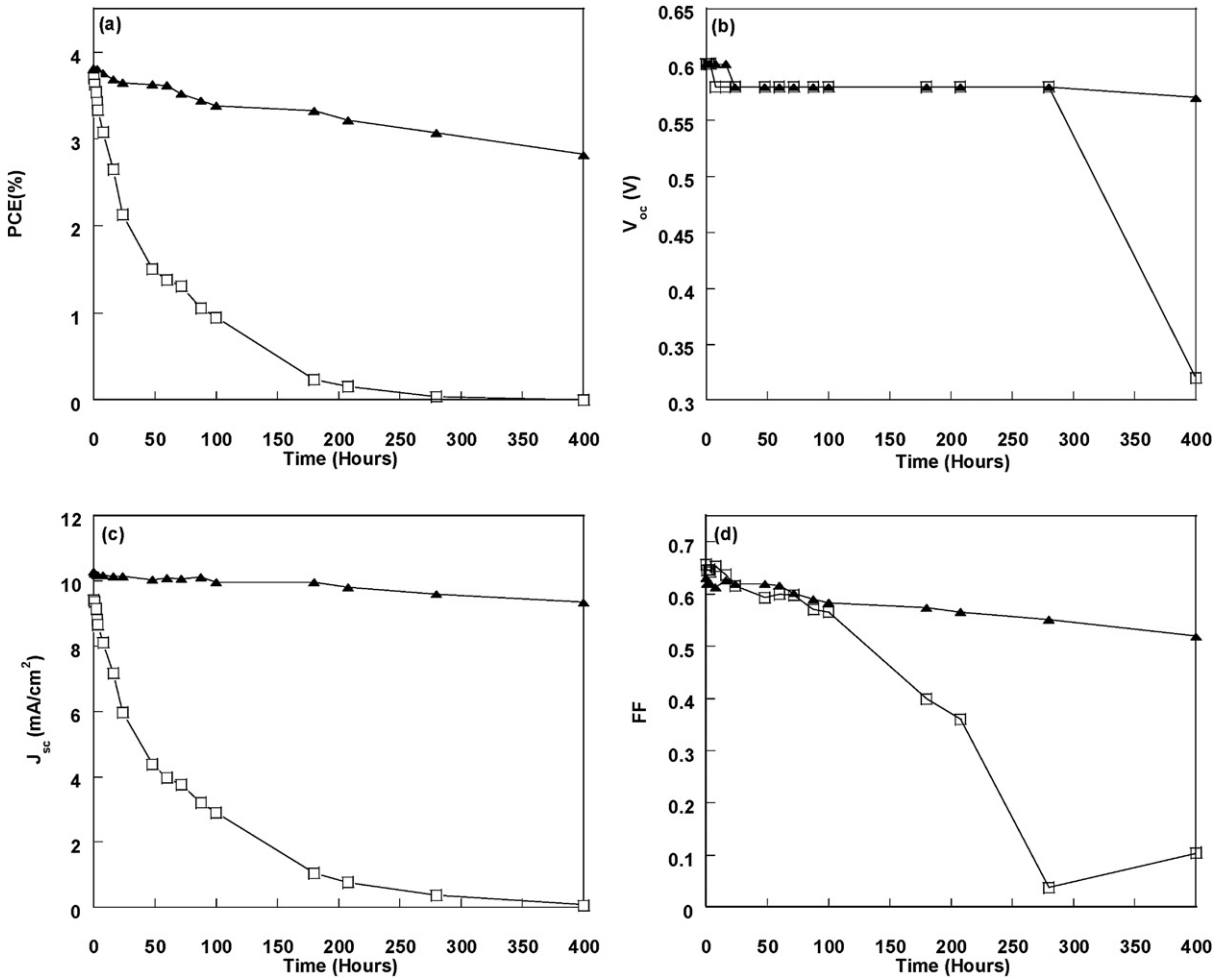

Fig. 5 Device parameters as a function of storage time for a conventional device (□) and an inverted device (▲): (a) power conversion efficiency (PCE), (b) open circuit voltage (V_{oc}), (c) short circuit current density (J_{sc}), and (d) fill factor (FF).

Acknowledgements

This research was supported by the National Science Council of Taiwan under grants NSC-96-2221-E-006-059, NSC-95-2221-E006-409-MY3, and NSC-96-2113-M- 006-009-MY3, and by the Asian Office of Aerospace Research and Development (AOARD-08-4076).

References

1 W. L. Ma, C. Y. Yang, X. Gong, K. Lee and A. J. Heeger, *Adv. Funct. Mater.*, 2005, **15**, 1617.
2 G. Li, V. Shrotriya, J. S. Huang, Y. Yao, T. Moriarty, K. Emery and Y. Yang, *Nat. Mater.*, 2005, **4**, 864.
3 J. Peet, J. Y. Kim, N. E. Coates, W. L. Ma, D. Moses, A. J. Heeger and G. C. Bazan, *Nat. Mater.*, 2007, **6**, 497.
4 A. M. Ballantyne, L. Chen, J. Nelson, D. D. C. Bradley, Y. Astuti, A. Maurano, C. G. Shuttle, J. R. Durrant, M. Heeney, W. Duffy and I. McCulloch, *Adv. Mater.*, 2007, **19**, 4544.
5 M. P. de Jong, L. J. van Ijzendoom and M. J. A. de Voigt, *Appl. Phys. Lett.*, 2000, **77**, 2255.
6 C. Waldauf, M. Morana, P. Denk, P. Schilinsky, K. Coakley, S. A. Choulis and C. J. Brabec, *Appl. Phys. Lett.*, 2006, **89**, 233517.
7 R. Steim, S. A. Choulis, P. Schilinsky and C. J. Brabec, *Appl. Phys. Lett.*, 2008, **92**, 093303.
8 M. S. White, D. C. Olson, S. E. Shaheen, N. Kopidakis and D. S. Ginley, *Appl. Phys. Lett.*, 2006, **89**, 143517.
9 H. H. Liao, L. M. Chen, Z. Xu, G. Li and Y. Yang, *Appl. Phys. Lett.*, 2008, **92**, 173303.
10 H. Ishii, K. Sugiyama, E. Ito and K. Seki, *Adv. Mater.*, 1999, **11**, 605.
11 A. Kahn, N. Koch and W. Gao, *J. Polym. Sci. B.*, 2003, **41**, 2529.
12 J. Huang, P. F. Miller, J. S. Wilson, A. J. de Mello, J. C. de Mello and D. D. C. Bradley, *Adv. Funct. Mater.*, 2005, **15**, 290.
13 C. Y. Li, T. C. Wen, T. F. Guo and S. S. Hou, *Polymer*, 2008, **49**, 957.
14 C. Y. Li, T. C. Wen and T. F. Guo, *J. Mater. Chem.*, 2008, **18**, 4478.
15 V. Shrotriya, G. Li, Y. Yao, T. Moriarty, K. Emery and Y. Yang, *Adv. Funct. Mater.*, 2006, **16**, 2016.
16 P. A. van Hal, M. M. Wienk, J. M. Kroon, W. J. H. Verhees, L. H. Slooff, W. J. H. van Gennip, P. Jonkheijm and R. A. J. Janssen, *Adv. Mater.*, 2003, **15**, 118.
17 V. D. Mihailetchi, P. W. M. Blom, J. C. Hummeien and M. T. Rispens, *J. Appl. Phys.*, 2003, **94**, 6849.
18 J. Gilot, M. M. Wienk and R. A. J. Janssen, *Appl. Phys. Lett.*, 2007, **90**, 143512.
19 H. Peisert, M. Knupfer, F. Zhang, A. Petr, L. Dunsch and J. Fink, *Appl. Phys. Lett.*, 2003, **83**, 3930.
20 H. Peisert, A. Petr, L. Dunsch, T. Chassé and M. Knupfer, *ChemPhysChem*, 2007, **8**, 386.
21 M. S. A. Abdou, F. P. Orifino, Y. Son and S. Holdcroft, *J. Am. Chem. Soc.*, 1997, **119**, 4518.
22 A. L. Linsebigler, G. Lu and J. T. Yates, Jr., *Chem. Rev.*, 1995, **95**, 735.
23 V. E. Henrich, P. A. Cox, *The surface Science of Metal Oxides*, Cambridge University Press, Cambridge, 1994.
24 C. Noguera, *Physics and chemistry of oxide surfaces*, Cambridge University Press, Cambridge, 1996.

ADVANCED FUNCTIONAL MATERIALS

FULL PAPER

DOI: 10.1002/adfm.200800403

Organic-Oxide Cathode Buffer Layer in Fabricating High-Performance Polymer Light-Emitting Diodes**

By *Tsung-Hsun Lee, Jung-Chun-Andrew Huang, Georgi L'vovich Pakhomov, Tzung-Fang Guo,* Ten-Chin Wen, Yi-Shun Huang, Chuan-Cheng Tsou, Chia-Tin Chung, Ying-Chang Lin,* and *Yao-Jane Hsu*

Spin-casting or thermal evaporation in vacuum of a salt-free, neutral, organic-oxide ultra-thin film as a buffer layer with an aluminum (Al) cathode has become an alternative approach for fabricating high-performance organic and polymer light-emitting diodes (O/PLEDs). [Guo et al., *Appl. Phys. Lett.* **2006**, *88*, 113501 and *Appl. Phys. Lett.* **2006**, *89*, 053507] The electroluminescence efficiency of phenyl-substituted poly(para-phenylene vinylene) copolymer-based PLEDs is 0.16 cd A^{-1} when Al is used as the device cathode, but is approximately two orders of magnitude higher, 14.53 cd A^{-1}, when an organic oxide/Al composite cathode is used. The polymer/metal junction in PLEDs with and without depositing an ultra-thin organic oxide interlayer is studied by X-ray photoelectron spectroscopy. Experimental results indicate that the deposition of an Al electrode causes the oxidation at the surface of the light-emissive polymer layer. Introducing an organic-oxide cathode buffer layer suppresses the oxidation and the diffusion of the Al atoms into the functional polymer layer. The formation of a carbide-like (negative carbon) thin layer, which accompanies interfacial interactions, is critical to the injection of electrons through the Al cathode. The balanced charge injection is responsible for the substantially improved device performance. This process is specific to the organic oxide/Al interface, as revealed by a comparison with similar device configurations that have Ag as the electrode, in which no significant interaction in the interface is observed.

1. Introduction

Aluminum (Al) is frequently used as electrodes in fabricating organic electronic devices, including organic/polymer light-emitting diodes (O/PLEDs),[1–3] organic photovoltaic or solar cells[4–6] and organic thin-film transistors.[7–9] However, the surface of Al, which intrinsically has a very large amount of non-bonding orbitals (dangling bonds) or surface states, is very active, oxidizing immediately when exposed to the atmosphere and tending to react with organic materials during vacuum thermal evaporation.[10,11] Additionally, the release of energy of Al followed by the condensation of metallic vapor on the substrate of organic/polymer film at room temperature breaks chemical bonds. Changes in the polymer configuration affect the overall performance of the devices and have stimulated the interest of many researchers.[12–16] Adding a thin layer of the inorganic salts, such as lithium fluoride (LiF) (<1 nm)[3,17,18] and cesium carbonate (Cs_2CO_3),[19] ionomers[20] or organic salts that contain Li or calcium (Ca) ions[21,22] in the cathode interface prevents an unfavorable interaction of Al with the functional organic layer, significantly improving the efficiency of O/PLEDs.

Our recent works have demonstrated a marked improvement in the electroluminescence (EL) efficiency of ''high-yellow'' phenyl-substituted poly (para-phenylene vinylene) copolymer (HY-PPV)-based PLEDs and tris-(8-hydroxyquinoline) aluminum-based OLEDs using the organic oxide/Al

[*] Dr. T.-F. Guo, Dr. G. L. Pakhomov
Institute of Electro-Optical Science and Engineering
Advanced Optoelectronic Technology Center, National Cheng Kung University
Tainan, Taiwan 701 (Republic of China)
E-mail: guotf@mail.ncku.edu.tw
T.-H. Lee, Dr. J. C. A. Huang
Department of Physics, Center for Micro/Nano Science and Technology
Institute of Innovations and Advanced Studies, National Cheng Kung University
Tainan, Taiwan 701 (Republic of China)
Dr. T.-C. Wen, Y.-S. Huang
Department of Chemical Engineering, National Cheng Kung University
Tainan, Taiwan 701 (Republic of China)
Dr. C.-C. Tsou, Dr. C.-T. Chung
Chi Mei Optoelectronics Corporation, Tainan Science-Based Industrial Park
Taiwan, 741, (Republic of China)
Y.-C. Lin, Dr. Y.-J. Hsu
National Synchrotron Radiation Research Center
Hsinchu, Taiwan 30076, (Republic of China)

[**] The authors would like to thank the National Science Council (NSC) of Taiwan (NSC96-2113-M-006-009-MY3) and the Asian Office of Aerospace Research and Development (AOARD-08-4076) for financially supporting this research. Dr. Pakhomov is on leave from Russian Academy of Sciences, Institute for Physics of Microstructures, N. Novgorod, Russia. Dr. Ruei-Tang Chen from Eternal Chemical Co., Ltd is highly appreciated for providing the HY-PPV polymer. The technical assistance from Center for Micro-NanoTechnology of National Cheng Kung University is also appreciated.

ADVANCED FUNCTIONAL MATERIALS

composite cathode.[23–26] Salt ions need not to be added to the cathode buffer layer.[23–29] Introducing a thin layer of ethylene-oxide derivative into the cathode interface of O/PLEDs facilitates the injection of electrons through the Al cathode and inhibits the metal-induced quenching sites of luminescence in the light-emissive layer near the recombination zone. Additionally, the organic oxide film somewhat blocks the excitons from the metal cathode, increasing the probability of radiative recombination. In this work, the interfacial properties at the polymer/metal junction in PLEDs with and without the deposition of an ultra thin organic-oxide interlayer are studied by X-ray photoelectron spectroscopy (XPS). The vacuum thermal deposition of Al is suggested to oxidize the surface of the conjugated polymer, where introducing an ultra-thin (2–5 nm) organic-oxide buffer layer at the polymer/metal junction suppresses the oxidation of the HY-PPV. The formation of a carbide-like layer at the junction interface, which is characterized by the XPS, accompanies the interfacial reaction and is important in facilitating the injection of electrons through the Al electrode. The EL efficiency of PLED made of HY-PPV as the light-emissive layer with Al as the cathode is 0.16 cd A^{-1}, but an organic oxide/Al composite cathode increases this value by approximately two orders of magnitude to 14.53 cd A^{-1}. The improved device performance follows essentially the specific interaction of Al with ethylene-oxide groups, $(–CH_2CH_2O–)_n$. When silver (Ag) is used instead of Al with the organic-oxide layer as the electrode, no significant interaction occurs in the polymer/metal junction and no improvement in the device performance is observed.

2. Results and Discussion

Figure 2 plots the normalized and corrected C 1s core level spectra from pristine HY-PPV, HY-PPV/Al50, HY-PPV/PEGDE25, HY-PPV/PEGDE25/Al50, and HY-PPV/PEGDE100/Al50 surfaces. The C 1s core level spectrum of the pristine HY-PPV surface has a main peak at a binding energy (BE) of 284.5 eV and a second peak at 286.0 eV. These peaks are associated with hydrocarbon atoms (C–C and C–H) and carbon atoms attached to the oxygen (C–O) of HY-PPV molecules, respectively. The deposition of the Al layer alters the chemical environment of carbon atoms at the surface of HY-PPV polymer, changing the relative intensity and chemical shifts in the spectra (HY-PPV/Al50 sample). However, the deposition of an ultra thin (25 Å) PEGDE layer on the HY-PPV surface has little or no effect on the profile of the C 1s line (HY-PPV/PEGDE25 sample), although the C–C/C–O peak ratio is different for PEGDE and HY-PPV polymers based on the chemical structures as shown in the Figure 1. The absence of any major change in the XPS spectra can be understood as following from the much lower actual thickness of the PEGDE layer than that of HY-PPV, but the presence of PEGDE in the interface is clearly manifest in the *I–L–V* characteristics of the device.

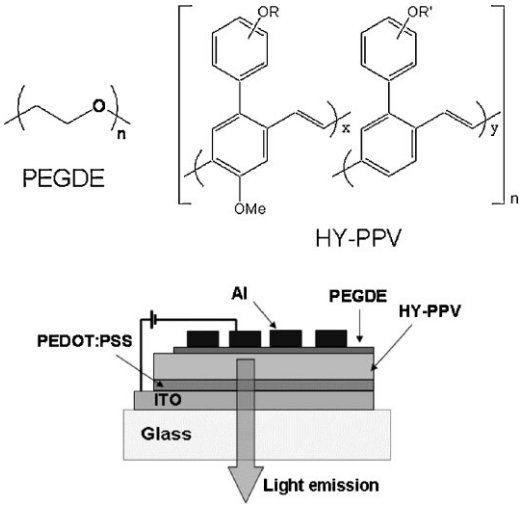

Figure 1. The chemical structure of PEGDE and HY-PPV, and the configuration of PLED presented in this study.

Figure 3a–d present deconvolutions of the C 1s core level signals as shown in Figure 2, based on the minimum Gaussian peaks to yield the best fit after the background subtraction.[32] In Figure 3a, peaks #2 (284.5 eV) and #3 (286.0 eV) of the pristine HY-PPV are associated with hydrocarbon atoms (C–C and C–H) and carbon atoms attached to the oxygen (C–O) of HY-PPV molecules, discussed in the above paragraph, respectively. The #4 (287.9 eV) peak is tentatively attributed to C=O bonds and the #5 (288.5 eV) peak is assigned to the carbon atoms in a highly oxidative environment, such as those in carboxylate ester groups.[33–35] The intensity of peaks #4 and #5 in Figure 3a is low, suggesting some unintentional oxidation or contamination of the polymer surface. In Figure 3c and d, the #1 (283.1 eV) peak is observed for the HY-PPV films on which had been deposited PEGDE and Al. The binding energies of carbon atoms in this range typically correspond to the carbide-like bonds.[15] The origin or formation of the carbide-like carbons is probably correlated with the interaction between the PEGDE buffer film and Al, as will be discussed below.

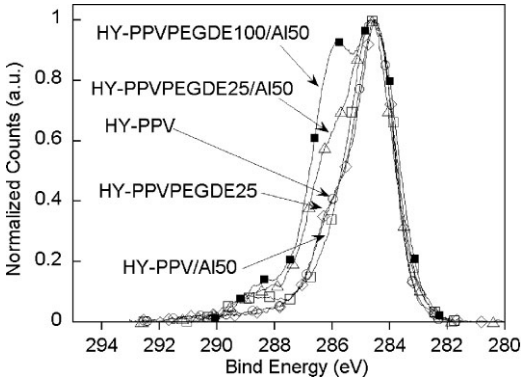

Figure 2. The normalized and corrected C 1s core level spectra obtained from (○) pristine HY-PPV, (□) HY-PPV/Al50, (◇) HY-PPV/PEGDE25, (△) HY-PPV/PEGDE25/Al50, and (■) HY-PPV/PEGDE100/Al50 surfaces.

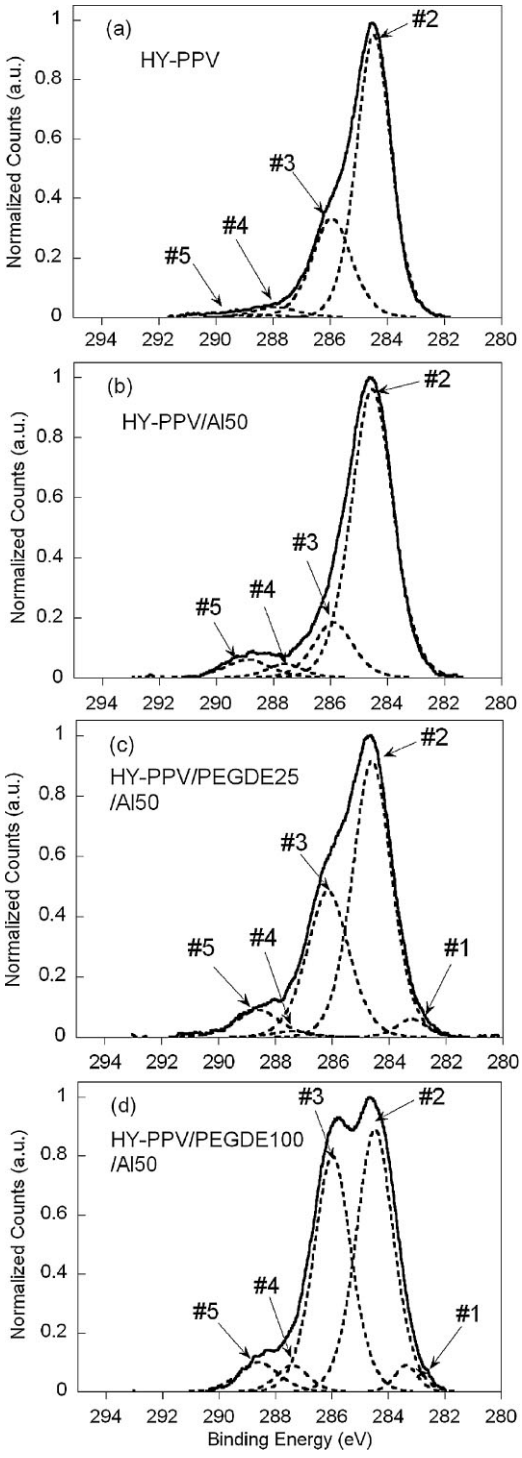

Figure 3. The deconvolutions of the normalized and corrected C 1s core level signals from a) HY-PPV, b) HY-PPV/Al50, c) HY-PPV/PEGDE25/Al50, and d) HY-PPV/PEGDE100/Al50 surfaces.

In Figure 3b, the evaporation of a thin Al layer on an HY-PPV surface changes the relative ratio of the intensities of the deconvoluted peaks and increases the intensity of the high-energy tail in the C 1s core level spectrum above that in Figure 3a. The intensity of the #3 peak in Figure 3b is approximately halve, which halving accompanied by a relative increase in the #2 peak (C–C and C–H bond). This result supports the assertion that some C–O bonds at the HY-PPV surface break following the deposition of the Al layer.[36] Furthermore, the marked increase in the intensity of the #5 peak above that in Figure 3b to a, associated with electron-deficient carbons, indicates the oxidation of the conjugated polymer.[33–35] Very likely, many $^{benzene}C–O–C^{alkyl}$ groups are transformed to the ester moieties by the addition of the second (carbonyl) oxygen to the C^{alkyl}-atom that is directly attached to the oxo-bridge in the side chain of HY-PPV. As a result, the high electron affinity of oxygen atoms causes a large chemical shift of ~4.0 eV in the C 1s core level spectrum, which is reasonably consistent with the literature.[33,34] The carbonyl-containing moieties and/or various oxidizing defects in poly(phenylene vinylene) (PPV)-based polymers are known to be the quenching sites for electroluminescence.[37–39] The oxidized interface is also expected to raise the series resistance of the devices, causing the low EL efficiency of PLEDs.

When a thin layer of Al is deposited on the surface of HY-PPV covered with an ultrathin 25 Å or 100 Å PEGDE layer for XPS measurement, the ~50 Å Al metal layer interferes with the penetration of the incident X-rays. The excited photo-electrons that are carried with the C 1s core level signals mainly escape from the PEGDE-rich region located directly beneath the Al layer. The PEGDE film has a higher C–O bond ratio than the HY-PPV film. As a result, in Figure 3c, the relative intensity of the #3 peak is higher than that of Figure 3a, partially because of the change in the XPS probing depth. The intensity of the #3 peak in Figure 3d is even larger than that in Figure 3c because of the better coverage of the thicker (100 Å) PEGDE layer on the HY-PPV surface, as also suggested by a decline in the full-width-half-maximum (FWHM) of the #3 peak in Figure 3d. The #5 peak regarding to highly oxidized ester-like carbon species presented in Figure 3b is still observed in Figure 3c and d, suggesting oxidation at the surface of the PEGDE-rich region induced by the deposited Al layer. Noticeably, the #1 peak at 283.1 eV is observed in both Figure 3c and d, revealing that the formation of a carbide-like thin layer at the interface is accompanied by an interaction between PEGDE and Al. The reaction of the PEGDE layer with the thermally evaporated Al probably suppresses the diffusion of Al into the HY-PPV layer, potentially inhibiting further oxidization or generation of metal-induced EL quenching sites in the HY-PPV layer near the recombination zone.[40–42] Figure 4 schematically presents; (a) the diffusion of Al atoms into the HY-PPV layer during vacuum thermal deposition; (b) the inhibition of diffusion of Al atoms by the PEGDE buffer at the polymer/meal junction.

Figure 5 presents the deconvoluted XPS spectra around the Al 2p peak obtained from the HY-PPV/PEGDE25/Al50 surface. A peak of metallic Al at 71.3 eV with a typically low FWHM is clearly observed in Figure 5. The broad peak at ~ 74.0 eV indicates that most Al atoms in the interface are in the form of some undetermined complex with oxygen (Al_xO_y).

ADVANCED FUNCTIONAL MATERIALS

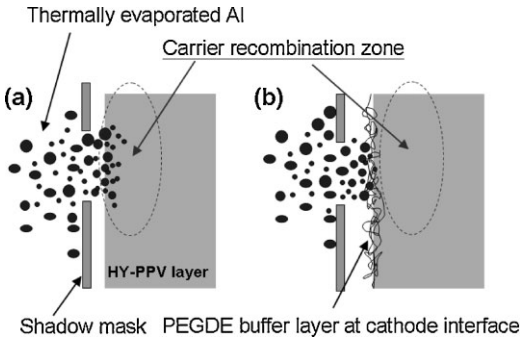

Figure 4. A schematic plot presents; a) the diffusion of Al atoms into the HY-PPV layer during vacuum thermal deposition; b) the inhibition of diffusion of Al atoms by the PEGDE buffer at the polymer/meal junction. The "cleaner" excitons recombination zone is expected in (b).

This result is consistent with the data published in the literature on an ultra-thin Al film that was thermally evaporated on a polymer surface under similar conditions.[11–13] The deconvolution of the Al 2p peak from the HY-PPV/PEGDE25/Al50 surface reveals the presence of two additional peaks – one at 75.4 eV, which corresponds to the oxide species, and the other one at 72.5 eV. The latter peak is at a position that is typically assigned to C-O-Al or C-Al bonds,[11,43,44] supporting the formation of carbide-like species revealed by the C 1s spectra in Figure 3c and d.

Devices that were fabricated with the same geometry and under identical conditions, but using Ag rather than Al as the metal electrode, were prepared for comparison. Figure 6 presents the normalized and deconvoluted C 1s core level spectra obtained from HY-PPV/Ag50, HY-PPV/PEGDE25/Ag50, and HY-PPV/PEGDE100/Ag50 surfaces. The best fittings obtained after the deconvolution of the XPS spectra are comprised of only three peaks. The peaks #1 and #5, which correspond to the carbide-like and highly oxidized ester-like carbon species, respectively, as observed in Figure 3, cannot be extracted in Figure 6. The ratio of C–C (#2 peak) to C–O (#3 peak) bonds gradually declines from HY-PPV/Ag50, HY-PPV/PEGDE25/Ag50 to HY-PPV/PEGDE100/Ag50, accompanying an increase in PEGDE content. The increase in the area of the #3 peak (C–O) in Figure 6b and c is substantially larger than that in Figure 3c and d, implying the minimal interaction of the thermally evaporated Ag layer with the polymers (PEGDE and HY-PPV). Additionally, the characteristic Ag 4d doublet in the range of 365–375 eV, commonly used to analyze the chemical shifts in Ag atoms,[35] does not exhibit any variation in the intensity or peak position. (Data not shown herein.) Those results imply that the carbide-like species are only generated at the PEGDE/Al interface.

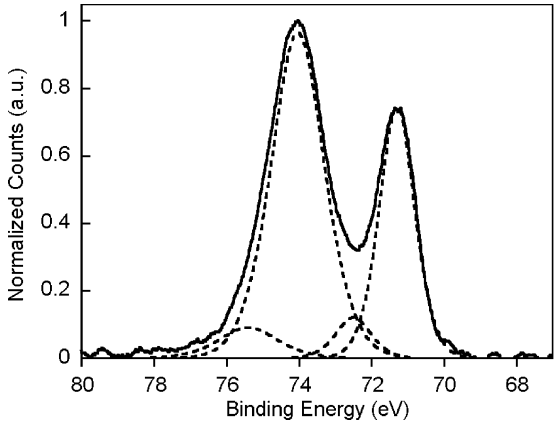

Figure 5. The deconvolution of the normalized and corrected Al 2p peak obtained from HY-PPV/PEGDE25/Al50 surface.

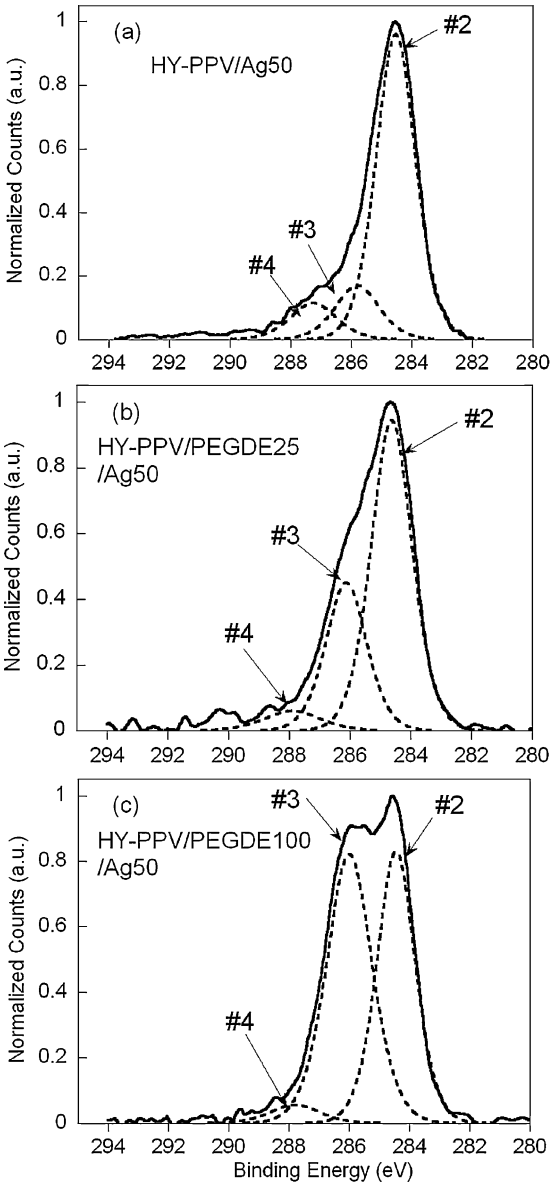

Figure 6. The deconvolution of the normalized and corrected C 1s core level spectra obtained from a) HY-PPV/Ag50, b) HY-PPV/PEGDE25/Ag50, and c) HY-PPV/PEGDE100/Ag50 surfaces.

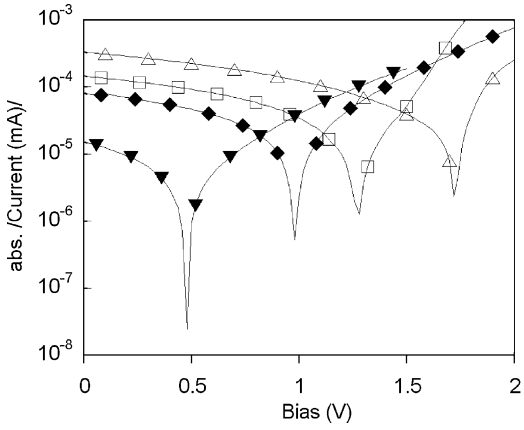

Figure 7. The photovoltaic measurements of (□) HY-PPV/Al800, (△) HY-PPV/PEGDE25/Al800, (◆) HY-PPV/Ag800, and (▼) HY-PPV/PEGDE25/Ag800 devices.

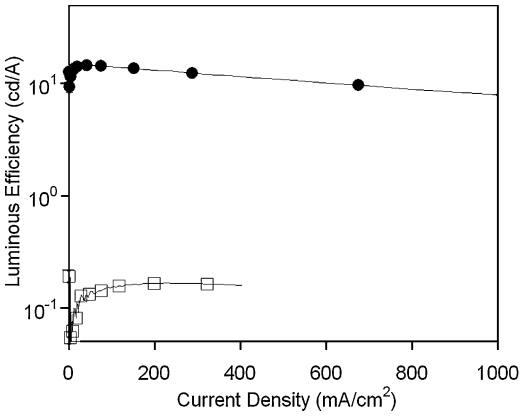

Figure 9. The luminous efficiency versus current density of (□) HY-PPV/Al800 and (●) HY-PPV/PEGDE45/Al800 devices.

The carbide-like (negative carbon) thin layer is essential to the formation of the interfacial dipoles or the decline in the metal work function of the electrode. Figure 7 shows the photovoltaic measurements for HY-PPV/Al800, HY-PPV/PEGDE25/Al800, HY-PPV/Ag800 and HY-PPV/PEGDE25/Ag800 devices. The open-circuit voltages (V_{oc}) of HY-PPV/Al800 and HY-PPV/PEGDE25/Al800 devices were ~1.25 V and ~1.72 V, respectively. This result suggests that the PEGDE buffer layer is responsible for the increase in the built-in potential of the HY-PPV/PEGDE/Al800 device, which implies a drop in the work function of PEGDE/Al cathode or the generation of interfacial dipoles at the polymer/metal junction.[22,24,27,28] However, the V_{oc} of the HY-PPV/PEGDE/Ag800 device is ~0.48 V – even lower than that of the HY-PPV/Ag800 device, ~0.98 V. This result indicates that the PEGDE is most likely an insulating layer, when incorporated with an Ag electrode.

The performance of HY-PPV-based PLED is optimized at a PEGDE buffer layer thickness of 45 Å with an Al cathode (HY-PPV/PEGDE45/Al800 device). Figure 8 plots the *I–L–V* curves of HY-PPV/Al800 and HY-PPV/PEGDE45/Al800 devices. The EL intensity of the HY-PPV/PEGDE45/Al800 device exceeds 85,000 cd m^{-2} when biased at ~10.0 V. The maximum luminous efficiency is approximately 14.53 cd A^{-1} at 6.80 V, 7794.02 cd m^{-2}. However, the EL intensity of the HY-PPV/Al800 device biased at ~10.0 V is only 641.80 cd m^{-2} and the maximum luminous efficiency is ~0.16 cd A^{-1} at 8.61 V, 288.44 cd m^{-2}. Moreover, the light turn-on voltage of the HY-PPV/PEGDE45/Al800 device was reduced to ~2.50 V from the corresponding value of the HY-PPV/Al800 device, which was about 3.50 V. This result also infers that the voltage for the effective injection of minority carriers was brought forward to the lower electrical bias, in which the shift results from the interfacial dipoles or the decline in the metal work function when the PEGDE buffer layer is introduced at the HY-PPV/Al junction. Figure 9 plots the luminous efficiency versus current density of HY-PPV/Al800 and HY-PPV/PEGDE45/Al800 devices. The luminous efficiency of HY-PPV/PEGDE45/Al800 device (~14.5 cd A^{-1}) is about two orders of magnitude higher than that of HY-PPV/Al800 device (~0.16 cd A^{-1}) and still remains high and stable when the devices are biased at high current and high brightness regime. Figure 10 displays the EL spectrum of the HY-PPV/PEGDE45/Al800 device. No

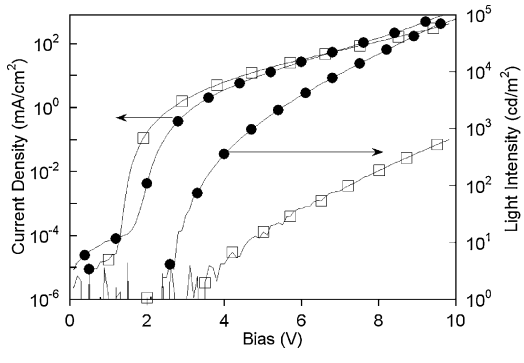

Figure 8. *I–L–V* curves of (□) HY-PPV/Al800 and (●) HY-PPV/PEGDE45/Al800 devices.

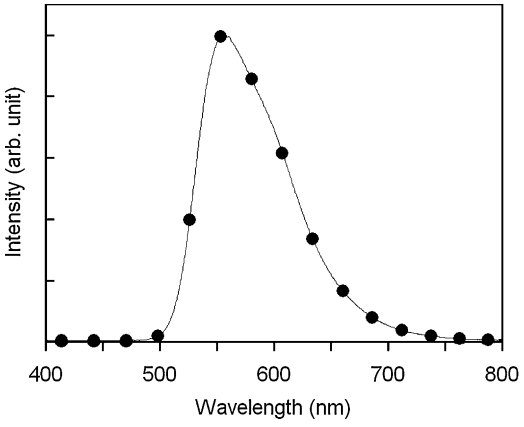

Figure 10. EL spectrum of HY-PPV/PEGDE45/Al800 device. No variation in the EL spectra or the CIE coordinates was observed at varied bias conditions.

variation in the EL spectra or the CIE coordinates was observed as the bias was varied. The high EL intensity and luminous efficiency of the HY-PPV/PEGDE45/Al800 device are attributable to the efficient injection of electrons through the cathode and the effective inhibition of the metal-induced EL quenching sites in the HY-PPV layer.

The above findings show that the organic-oxide buffer layer markedly improved the overall device performance. However, further increasing the thickness of the PEGDE interlayer to 100 Å degrades the device performance. The series resistance of the device limits the injection of charge carriers through the Al cathode because the PEGDE film is intrinsically insulating. Our earlier publication presented that the device performance changes with the thickness of the PEGDE buffer layer.[24]

3. Conclusion

In summary, the modification of a bare conjugated polymer surface by the thermal deposition of an Al cathode is rather complicated. This study demonstrates the oxidation of both the surface of the conjugated polymer and the Al metallic layer upon the thermal evaporation of Al cathode occurs in a vacuum (10^{-6} Torr). The oxidation substantially worsens the performance of PLEDs, but can be suppressed by applying an ultra-thin PEGDE buffer layer at the HY-PPV/Al interface. The polymer/metal junctions of HY-PPV-based PLEDs with and without introducing the PEGDE buffer layer are investigated by the high-resolution XPS. The formation of an ultra-thin Al-C interlayer, which accompanies the interaction of thermally evaporated Al with the PEGDE buffer layer, is presumed to be based on the C 1s and Al 2p core level spectra. The specific organic oxide/Al complex at the cathode interface effectively facilitates the injection of electrons through the Al electrode at a low bias voltage and also suppresses the formation of metal-induced EL quenching sites in the HY-PPV layer. The use of the PEGDE/Al cathode improves the EL intensity and luminous efficiency of HY-PPV-based PLED by approximately two orders of magnitude over those when Al is used as the device cathode. The balanced charge injection and probably the high radiative recombination efficiency in the active layer of HY-PPV/PEGDE45/Al800 device contribute to the enhanced EL efficiency. This work discussed the origins of the functionalized organic-oxide buffer layer in the fabrication of high-performance PLEDs: the steps for preparing the salt-free, neutral interfacial layer can be easily integrated into the manufacturing procedure.

4. Experimental

Fabrication of PLEDs: The device configuration, as shown in Figure 1, comprises indium-tin-oxide (ITO)/glass substrate as the anode, poly(3,4-ethylenedioxythiophene):polystyrenesulfonate (PEDOT:PSS Bayer Corp. 4083) as the hole transport layer, HY-PPV film as the light-emissive layer (~850 Å) [31], organic-oxide polymer as the interface buffer layer and the metal cathode electrode. The details for the fabrication of typical PLEDs can also be found elsewhere [24]. The organic-oxide film is prepared by thermally evaporating a thin polymer layer of poly(ethylene glycol) dimethyl ether (PEGDE) (Aldrich, M_n ca. 2,000) onto the surface of the HY-PPV film inside a vacuum chamber (10^{-6} Torr). The metal electrode is then evaporated on the substrates without breaking the vacuum. The thickness of the thermally evaporated PEGDE and the metal layers are determined by the quartz crystal thickness monitor inside the vacuum chamber. The active pixel area of the device is 0.06 cm^2. The chemical structures of PEGDE and HY-PPV are also presented in Figure 1.

The Current–Brightness–Voltage and Photovoltaic Measurement of PLEDs: The current-brightness-voltage (*I–L–*V) measurements are made using a Keithley 2400 source measuring unit and a Keithley 2000 digital multimeter, along with a silicon photodiode, calibrated by a Minolta LS-100 luminosity meter. The photovoltaic measurement is performed under the illumination supplied by a Thermo Oriel 300 W solar simulator (AM 1.5G). All of the steps, except for casting the PEDOT:PSS layer, are implemented inside a nitrogen-filled glove box.. The sample configurations of the ITO/PEDOT:PSS/HY-PPV/Al(800 Å) (HY-PPV/Al800 device), ITO/PEDOT:PSS/HY-PPV/PEGDE(25 Å)/Al(800 Å) (HY-PPV/PEGDE25/Al800 device), ITO/PEDOT:PSS/HY-PPV/Ag(800 Å) (HY-PPV/Ag800 device) and ITO/PEDOT:PSS/HY-PPV/PEGDE(25 Å)/Ag(800 Å) (HY-PPV/PEGDE25/Ag800 device) are prepared for the photovoltaic measurement.

XPS Measurement: The interfacial properties of the polymer/metal junction is studied by the XPS measurements, which are done by a VG CLAM4 surface analysis system, equipped with an Al Kα radiation (1486.6 eV) at the National Synchrotron Radiation Research Center, Taiwan. The base pressure for the XPS measurement is below 8×10^{-10} Torr and the energy step is 0.025 eV. The sample configurations of the ITO/PEDOT:PSS/HY-PPV (HY-PPV sample), ITO/PEDOT:PSS/HY-PPV/Al(50 Å) (HY-PPV/Al50 sample), ITO/PEDOT:PSS/HY-PPV/PEGDE(25 Å) (HY-PPV/PEGDE25 sample), ITO/PEDOT:PSS/HY-PPV/PEGDE(25 Å)/Al(50 Å) (HY-PPV/PEGDE25/Al50 sample), and ITO/PEDOT:PSS/HY-PPV/PEGDE(100 Å)/Al(50 Å) (HY-PPV/PEGDE100/Al50 sample) are prepared for the XPS measurement. Additionally, Ag is used instead of Al to prepare another set of samples with the identical configurations for the comparison in the XPS measurement. The size of each sample for XPS measurement is around 1.0×1.0 cm^2.

Received: March 21, 2008
Published online: September 22, 2008

[1] D. Braun, A. J. Heeger, *Appl. Phys. Lett.* **1991**, *58*, 1982.
[2] C. W. Tang, S. A. VanSlyke, *Appl. Phys. Lett.* **1987**, *51*, 913.
[3] L. S. Huang, C. W. Tang, M. G. Mason, *Appl. Phys. Lett.* **1997**, *70*, 152.
[4] H. Hoppe, N. S. Sariciftci, *J. Mater. Chem.* **2006**, *16*, 45.
[5] C. J. Brabec, N. S. Sariciftci, J. C. Hummelen, *Adv. Funct. Mater.* **2001**, *11*, 15.
[6] G. Yu, J. Gao, J. C. Hummelen, F. Wudl, A. J. Heeger, *Science* **1995**, *270*, 1789.
[7] C. W. Chu, S. H. Li, C. W. Chen, V. Shrotriya, Y. Yang, *Appl. Phys. Lett.* **2005**, *87*, 193508.
[8] S. H. Li, Z. Xu, L. Ma, C. W. Chu, Y. Yang, *Appl. Phys. Lett.* **2007**, *91*, 083507.
[9] T. F. Guo, Z. J. Tsai, S. Y. Chen, T. C. Wen, C. T. Chung, *J. Appl. Phys.* **2007**, *101*, 124505.
[10] P. Dannetun, M. Logdlund, M. Fahlman, M. Boman, S. Stafstrom, W. R. Salaneck, R. Lazzaroni, C. Fredriksson, J.-L. Brédas, S. Graham, R. H. Friend, A. B. Holmes, R. Zamboni, C. Talliani, *Synth. Met.* **1993**, *55*, 212.
[11] T. P. Nguyen, J. Ip, P. Jolinat, P. Destruel, *Appl. Surf. Sci.* **2001**, *172*, 75.

[12] W. J. H. van Gennip, J. K. J. van Duren, P. C. Thune, R. A. J. Janssen, J. W. Niemantsverdriet, *J. Chem. Phys.* **2002**, *117*, 5031.
[13] A. Crispin, A. Jonsson, M. Fahlman, W. R. Salaneck, *J. Chem. Phys.* **2001**, *115*, 5252.
[14] G. G. Andersson, W. J. H. van Gennip, J. W. Niemantsverdriet, H. H. Brongersma, *Chem. Phys.* **2002**, *278*, 159.
[15] R. Sutcliffe, W. W. Lee, J. F. Gaynor, J. D. Luttmer, D. Martini, J. Kelber, M. A. Plano, *Appl. Surf. Sci.* **1998**, *126*, 43.
[16] L. Sandrin, E. Sacher, *Appl. Surf. Sci.* **1998**, *135*, 339.
[17] G. E. Jabbour, Y. Kawabe, S. E. Shaheen, J. F. Wang, M. M. Morrell, B. Kippelen, N. Peyghambarian, *Appl. Phys. Lett.* **1997**, *71*, 1762.
[18] J. Yoon, J. J. Kim, T. W. Lee, O. O. Park, *Appl. Phys. Lett.* **2000**, *76*, 2152.
[19] J. Huang, Z. Xu, Y. Yang, *Adv. Funct. Mater.* **2007**, *17*, 1966.
[20] T. W. Lee, O. O. Park, L. M. Do, T. Zyung, T. Ahn, H. K. Shim, *J. Appl. Phys.* **2001**, *90*, 2128.
[21] Y. Cao, G. Yu, A. J. Heeger, *Adv. Mater.* **1998**, *10*, 917.
[22] Q. Xu, J. Ouyang, Y. Yang, T. Ito, J. Kido, *Appl. Phys. Lett.* **2003**, *83*, 4695.
[23] T. F. Guo, F. S. Yang, Z. J. Tsai, T. C. Wen, S. N. Hsieh, Y. S. Fu, *Appl. Phys. Lett.* **2005**, *87*, 013504.
[24] T. F. Guo, F. S. Yang, Z. J. Tsai, T. C. Wen, S. N. Hsieh, Y. S. Fu, C. T. Chung, *Appl. Phys. Lett.* **2006**, *88*, 113501.
[25] T. F. Guo, F. S. Yang, Z. J. Tsai, G. W. Feng, T. C. Wen, S. N. Hsieh, C. T. Chung, C. I. Wu, *Appl. Phys. Lett.* **2006**, *89*, 051103.
[26] T. F. Guo, F. S. Yang, Z. J. Tsai, T. C. Wen, C. I. Wu, C. T. Chung, *Appl. Phys. Lett.* **2006**, *89*, 053507.
[27] X. Y. Deng, W. M. Lau, K. Y. Wong, K. H. Low, H. F. Chow, Y. Cao, *Appl. Phys. Lett.* **2004**, *84*, 3522.
[28] Y. H. Niu, H. Ma, Q. Xu, A. K. Y. Jen, *Appl. Phys. Lett.* **2005**, *86*, 083504.
[29] J. H. Park, O. O. Park, J. W. Yu, J. K. Kim, Y. C. Kim, *Appl. Phys. Lett.* **2004**, *84*, 1783.
[30] K. Cho, S. W. Cho, C. N. Whang, K. Jeong, S. J. Kang, Y. Yi, *Appl. Phys. Lett.* **2007**, *91*, 152107.
[31] H. Becker, H. Spreitzer, W. Kreuder, E. Kluge, H. Schenk, I. Parker, Y. Cao, *Adv. Mater.* **2000**, *12*, 42.
[32] G. L. Pakhomov, L. G. Pakhomov, V. I. Shashkin, J. M. Tura, J. M. Ribo, L. Ottaviano, *Nucl. Instrum. Methods Phys. Res. Sect. B* **2002**, *194*, 269.
[33] C. C. Wang, G. H. Hsiue, *J. Polym. Sci. Part A* **1993**, *31*, 2601.
[34] M. Atreya, S. Li, E. T. Kang, K. G. Neoh, K. L. Tan, *Polym. Degrad. Stab.* **1999**, *63*, 53.
[35] N. Dam, M. M. Beerbom, J. C. Braunagel, R. Schlaf, *J. Appl. Phys.* **2005**, *97*, 024909.
[36] K. Konstadinidis, F. Papadimitrakopoulos, M. Galvin, R. L. Opila, *J. Appl. Phys.* **1995**, *77*, 5642.
[37] M. Yan, L. J. Rothberg, F. Papadimitrakopoulos, M. E. Galvin, T. M. Miller, *Phys. Rev. Lett.* **1994**, *73*, 744.
[38] R. H. Friend, R. W. Gymer, A. B. Holmes, J. H. Burroughes, R. N. Marks, C. Taliani, D. D. C. Bradley, D. A. Dos Santos, J.-L. Brédas, M. Lögdlund, W. R. Salaneck, *Nature* **1999**, *397*, 121.
[39] D. R. Baigent, A. B. Holmes, S. C. Moratti, R. H. Friend, *Synth. Met.* **1996**, *80*, 119.
[40] H. Becker, A. Lux, A. B. Holmes, R. H. Friend, *Synth. Met.* **1997**, *85*, 1289.
[41] H. Becker, S. E. Burns, R. H. Friend, *Phys. Rev. B* **1997**, *56*, 1893.
[42] P. W. M. Blom, M. C. J. M. Vissenberg, J. N. Huiberts, H. C. F. Martens, H. F. M. Schoo, *Appl. Phys. Lett.* **2000**, *77*, 2057.
[43] T. P. Nguyen, J. L. Mansot, *Thin Solid Films* **1996**, *283*, 135.
[44] S. J. Ding, Q. Q. Zhang, D. W. Zhang, J. T. Wang, Y. D. Zhou, W. W. Lee, *Appl. Surf. Sci.* **2001**, *178*, 140.

Correlation of excited states with magneto conductance response in polymer photovoltaic devices

Tsung-Hsun Lee[1], Bin Hu[2], Cheng-Lun Tsai[1], Ruei-Syuan Guan[3],
Tzung-Fang Guo [a), 3], J. C. A. Huang [b), 4]

[1]Department of Physics,
National Cheng Kung University
Tainan, Taiwan 701, Republic of China

[2]Department of Materials Science and Engineering
University of Tennessee
Knoxville, Tennessee 37996,USA

[3]Institute of Electro-Optical Science and Engineering
Advanced Optoelectronic Technology Center
National Cheng Kung University
Tainan, Taiwan 701, Republic of China

[4]Department of Physics,
Center for Micro/Nano Science and Technology,
Institute of Innovations and Advanced Studies,
National Cheng Kung University
Tainan, Taiwan 701, Republic of China

Abstract

This study elucidates the influence of applied magnetic filed, electrical bias and the

[a)] Author to whom all correspondence should be addressed; electronic mail: guotf@mail.ncku.edu.tw

[b)] Author to whom all correspondence should be addressed; electronic mail: jcahuang@mail.ncku.edu.tw

different device electrode on the dissociation, intersystem crossing, and charge reaction processes of photo- and electrical-induced excited states in regioregular poly(3-hexylthiophene) (P3HT)-based polymer photovoltaic devices. The dissociation of the singlet polaron-polaron (PP) pairs, as facilitated by the applied magnetic field, is responsible for a positive magneto conductance (MC) effect. However, a negative MC effect is dominated by the decline of charge-reaction rates for triplet excitons. The net MC responses of the photovoltaic cells are basically the sum of the positive and negative MC effects, which can be manipulated by the applied magnetic field and electrical bias. An inversion in the MC response is observed at the electrical bias near the open-circuit voltage. In addition, blending of an electron acceptor material, [6,6]-phenyl C61-butyric acid methyl ester, in P3HT active layer quenches the photo-excited states at the donor-acceptor interface and results in distinct MC responses of photovoltaic cells, which probably are related to the features indicating the formation of intermolecular charge-transfer complexes at donor-acceptor junction.

1. Introduction

Organic conjugated molecules/polymers have very unique properties. [1-3] They can be used as organic semiconductors in fabricating novel electronic devices. [4-9] In addition, the electronic devices incorporating organic conjugated molecules/polymers as the active layers exhibit the strong magneto responses. [10, 11] The output performance, such as the electroluminescence, [10, 12-14] resistance or conductance, [10-16] and photocurrent [11, 17-20] in organic/polymer diodes and photovoltaic (PV) cells can be modulated by the applied magnetic field, although the basic device configurations are composed of intrinsically non-magnetic components. The magneto responses of organic semiconductors would have new applications in organic electronic and spintronic devices. [21-24]

A large magneto resistance (MR) or magneto conductance (MC) response in organic/polymer light-emitting diodes (O/PLEDs) has been reported by many researchers, which is intimately associated with the threshold of light emission and the ambipolar injection of charge carriers. [10, 25] While the organic/polymer diodes are operated at PV regime with illumination, the magnitude of photocurrent is varied with the applied magnetic field. [11, 17-20] These results suggest the dissociation and the charge-reaction processes of the photo-excited states that transform into free charge carriers are susceptible to change by the applied magnetic filed. The excited states, induced either electrically (in O/PLEDs) or optically (in PV cells), in organic semiconductor layers, are essentially important to the MR or MC responses in organic/polymer diodes and PV cells. [26-30]

The photo-induced excited states (excitons) in the regioregular poly(3-hexylthiophene) (P3HT)-based polymer diodes are Coulombically bound

electron-hole (e-h) pairs, commonly having a short range of separation distance. [27, 31-33] Those excitons may undergo a relaxation processes to become the excited polaron-polaron (PP) pairs with a longer range of the e-h separation distance than that of excitons. Figure 1(a) illustrates schemes for the formation of intra- and inter-molecular excited PP pairs from excitons. Both the excitons and PP pairs are the excited states of conjugated organic molecules processing singlet and triplet electronic configurations. The ratio of singlet/triplet can be changed through the intersystem crossing process as illustrated in Fig. 1(b). The magnitude of exchange energy for the singlet/triplet excited PP pairs is exponentially decayed with respect to the e-h separation distance. [30, 31] Accordingly, the status (or the singlet/triplet intersystem crossing rate) of the long-range (>1 nm) PP pairs having exchange energies of the order smaller than 10^{-3} meV is subjected to changes brought in by the applied magnetic field. Since the photocurrent of P3HT-based diodes is the sum of 'current flows' generated by the photo-excited states (excitons and PP pairs), any variations induced by an applied magnetic filed on the distribution, dissociation, and charge-reaction processes of the singlet/triplet excited states (excitons and PP pairs) would certainly modulate the magnitude of photocurrent and MC responses in PV devices, as reported by Xu *et al.*. [18, 30] In this manuscript, the influence of the applied magnetic filed, electrical bias, and different device electrode on the dissociation, intersystem crossing, and charge reaction processes of photo-induced excited states in P3HT-based polymer diodes is studied. The dissociation of the singlet PP pairs, as facilitated by the external magnetic field, is accountable for an increase of photo-generated free charge carriers and a positive MC effect. However, the decline of charge-reaction rates for triplet excitons, caused by the applied magnetic field, results in the decrease of photo-generated free charge carriers and contributes to a negative MC

effect. The net MC responses of the photovoltaic cells are the sum of positive and negative MC effects, which are varied with the applied magnetic filed and electrical bias. An inversion in MC response is observed at the electrical bias near the open-circuit voltage. The magneto responses for intermolecular charge-transfer complex states at the donor-acceptor interface are investigated by blending an electron acceptor material, [6,6]-phenyl C61-butyric acid methyl ester (PCBM), in P3HT as the active layer. The distinct MC features suggest the formation of intermolecular charge-transfer complexes at donor-acceptor junction.

2. Experimental

The polymer diodes and photovoltaic devices are fabricated in a standard arrangement by sandwiching the active layer between a transparent electrode and a metal electrode. The transparent electrode is comprised of the cleaned indium-tin-oxide (ITO) covered glass substrate (RITEK Corp., 15 Ω/□) coated with poly(3,4-ethylenedioxythiophene) poly(styrenesulfonate) (PEDOT:PSS; Baytron P, Bayer AG, Germany) layer. Regioregular organic P3HT (98.5% electronic grade, Rieke Metals, Inc., USA) and PCBM (procured from Nano-C, USA) are dissolved in dichlorobenzene to yield the P3HT (20 mg/ml) and P3HT:PCBM (20:20 mg/ml) solutions. The active layers are obtained by spin-coating the solutions on the PEDOT:PSS/ITO/glass substrates at the drying process of the films in a slow-growth regime. [35, 36] Ca (40 nm) and Al (100 nm), as metal electrodes, are thermally deposited onto the surface of the active layer inside a vacuum chamber ($3x10^{-6}$ torr).

A halogen lamp is used as the light source (80 mW/cm^2) to investigate the MC response of the photovoltaic cells in this study. The devices are encapsulated by the

UV-curable epoxy with a cover glass and placed at the direction parallel to the magnetic field. In order to eliminate the influence due to drifting with different bias voltages, the *J-V* curves are averaged, based on the approach reported by Desai *et al.*. [13] The MC magnitude presented in this manuscript is defined as;

$$MC = \frac{\Delta I(B)}{I(0)} = \frac{I(B) - I(0)}{I(0)} \qquad (1)$$

Where *I(B)* and *I*(0) are the current intensity of the photovoltaic cells with and without the applied magnetic field, respectively. All the measurements are performed at room temperature. The magneto conductance of polymer diodes in our study is found to be independent to the direction of the external magnetic field. [20] The schematic drawings of the device configuration and the measurement of MC responses in our studies are illustrated in Figure 2.

3. Result and Discussion

3.1 Applied magnetic field and device electrodes on MC responses

Figure 3 presents the measured MC of the short-circuit current (I_{sc}, photocurrent measured at 0V bias voltage) for devices with the configurations of ITO/PEDOT:PSS/P3HT/Al (P3HT/Al-device) and ITO/PEDOT:PSS/P3HT/Ca/Al (P3HT/Ca-device) with illumination. MC response of the I_{sc} for P3HT/Al-device is positive and sharply increased from 0% to 0.8% in the low magnetic field (<30 mT) and then gradually decreased as the applied magnetic field is increased. The MC of P3HT/Al-device is reduced to zero and inversed from positive to negative at the applied magnetic field near B~150mT, and is of ~-1.4% at B=900mT. The positive and negative MC response of the I_{sc} for P3HT/Al-device is modulated by the applied magnetic field.

Xu *et al.* suggested that a low magnetic field usually affects the formation rate of the singlet/triplet PP pairs at the relaxation processes of photo-induced excitons. [18, 30] The increased distribution of singlet PP pairs by the applied magnetic filed raises the I_{sc} (singlet PP pairs have a relatively higher dissociation rate for converting into free charge carriers than that of triplet PP pairs), [27, 19] and contributes a positive and sharply elevated MC response in the low magnetic field for P3HT/Al-device. However, as the applied magnetic filed is gradually increased, the decrease of the charge-reaction rates for triplet excitons simultaneously causes a reduction in the I_{sc}, which accounts for a negative MC response. As a consequence, the magnetic-field dependence of the I_{sc} for P3HT/Al-device can be attributed to the tradeoff between the distribution & dissociation of the singlet PP pairs (positive MC response) with that of charge-reaction rates for triplet excitons (negative MC response) under the influence of the applied magnetic field.

While the Ca is used instead of Al as the metal electrode for P3HT-based polymer diode, the MC curve of P3HT/Ca-device is negatively increased with the applied magnetic field (not like that of P3HT/Al-device), as show in Fig. 3. Since the interfacial barrier height at the polymer/metal junction is reduced by the low work function Ca electrode, P3HT/Ca-device has a better polymer/metal interface for the generation and collection of charge carriers than that of P3HT/Al-device as applied for photovoltaic cells. [37, 38] The higher dissociation or charge-reaction rates of photoexcited states in P3HT/Ca junction probably reduce the effect of applied magnetic field on the singlet PP pairs. Consequently, MC response of P3HT/Ca-device is dominated by the influence of the applied magnetic field on the change-reaction rates of triplet excitons (having the longer lifetime). The charge-reaction rates of triplet excitons are reduced as the applied magnetic filed is increased, which decreases the overall photocurrent and hence results in

the net negative MC responses. The MC of P3HT/Ca-device is of ~-4.0% in an applied magnetic field of B=1000mT.

The devices with the configuration of ITO/PEDOT:PSS/P3HT/LiF/Ca/Al (P3HT/LiF/Ca-device) are also fabricated to investigate the influence of the additional dipole layer at P3HT/Ca interface on MC responses. Figure 4 illustrates the MC curves of the I_{sc} for P3HT/LiF(X nm)/Ca-device with varied thicknesses of LiF layers. The measured MC responses of I_{sc} in an applied magnetic field of B=1000mT are of ~-4.0%, -2.9%, and -2.3% for P3HT/LiF(X nm)/Ca-device of X= 0, 1.5, and 5.0 nm, respectively. The magnitudes of MC responses decrease with increasing thickness of LiF layer. These results suggest that the additional dipole layer (LiF) functions as an internal electrical field to accelerate the dissociation of the photo-excited states near the polymer/metal junction, but lower the influence (reducing the charge-reaction rate) of the applied magnetic field on the triplet excitons. The inset of Fig. 4 presents the thickness of LiF layer versus MC response at B=1000mT and abs. I_{sc} plots. The magnitudes of abs. I_{sc} are increased with the thickness of interfacial dipole layer, which are of 0.007, 0.023, and 0.076 mA/cm^2 for P3HT/LiF(X nm)/Ca-device of X= 0, 1.5, and 5.0 nm, respectively, and are associated with the decreased magnitude of MC responses.

3.2 The electrical bias on MC responses

Figure 5(a) presents the MC curves of P3HT/Ca-device with illumination at the varied bias voltages. The MC responses are of ~-4.0% for the P3HT/Ca-device biased at 0.00 V and 0.50 V in an applied magnetic field of B=1000mT, and they significantly increase to ~-5.0% and ~-24.0% when the devices are biased at 0.90V and 1.00V, respectively. However, the MC response is reversed from negative (~-24.0% at 1.00V) to

positive (~ 2.0% at 1.10V) as the bias voltage was raised to 1.10V and is almost vanished (<0.1%) at a bias voltage that exceeds 1.50 V. Figure 5(b) plots the MC curve of the P3HT/Ca-device with illumination versus bias voltage and semi-logarithm current-voltage (*J*-*V*) plot at B=1000mT. The inversion of the MC curve is found at the bias voltage close to the V_{oc} in the semi-logarithm *J*-*V* plot.

The photoexcited states in P3HT active layer are the Coulombically bound e-h pairs. The Coulombic interaction of those excited e-h pairs is varied with the separation distance and is subjected to change with magnitude and direction of the internal (difference in the work function of two electrodes) and external (the applied bias) electrical field. As the applied bias voltage of P3HT/Ca-device approaches V_{oc}, the influence of the internal electrical filed on the Coulombically bound e-h pairs is minimized, because the internal electrical field is offset by the applied electrical bias. The internal and the external electrical fields are of opposite directions at the bias regime in which the applied voltage is lower than the V_{oc}. As a result, MC response of P3HT/Ca-device at the applied bias close to V_{oc} would be generally determined by the influence of the applied magnetic field on the photoexcited states, in which the mechanism for the decrease in charge-reaction rates of the triplet excited states is eminent as mentioned in the previous paragraph and thus results in the maximum (negative) MC response. In addition, the denominator *I(0)* in Eq. (1), which is approximately the sum of the device current under dark conditions (I_d) and the photocurrent (I_p) in the absence of a magnetic filed, is nearly zero as the bias voltage approaches V_{oc}. Figure 6 presents the energy diagrams of P3HT/Ca-device at the applied voltages below and above the V_{oc}. The flow directions of I_d and I_p are also plotted in the figures. I_d and I_p are of the opposite

directions before V_{oc}. The thermal effect to flip the electron spin of triplet excitons is minimized at the low device current regime (at the bias voltage close to V_{oc}), which probably also accounts for one of the parameters to show the maximum (negative) MC response of P3HT/Ca-device. Therefore, a drastic MC response (negative) as calculated by Eq. (1) at an applied bias voltage close to V_{oc} is observed as shown in Fig. 5(a) and (b).

The injection of charge carriers occurs at the bias voltage larger than V_{oc}. Firstly, *I(0)* (I_d plus I_p) is exponentially increased in this bias regime. Secondly, the excited states in P3HT active layer should include the electrical-induced excitons and PP pairs from the recombination of the injected and oppositely-charged carriers. The Coulombic interactions of those excited (photo- and electrical-induced) states may be reduced by the external electrical filed at the bias voltage larger than the V_{oc}, in which the dissociation and charge reaction processes of excited PP pairs are more susceptible to the applied magnetic filed and contribute to a net positive MC response. The MC curve is positively increased and inversed from ~-24.0% at 1.00V to ~ 2.0% at 1.10V, B=1000mT. However, the MC response is almost suppressed as the current densities or bias voltages increase. This result can be interpreted by that the current generated by the formation and dissociation of excited states under the influence of external magnetic filed only accounts for a relatively small amount of the total current density. The denominator *I(0)* is exponentially increased at the bias voltage larger than V_{oc}, which is responsible for a relatively small MC response based on the calculation in the Eq. (1). The thermal effect in the high current regime also flips the electron spin of triplet excitons and reduces the influence of applied magnetic field on the excited states. The above summaries fortify the assumption that the measured MC is basically associated with the interaction of excited

states with the applied magnetic field and electrical bias.

3.3 Features of intermolecular charge-transfer complexes on MC responses

Figure 7 illustrates the MC curves of P3HT/Ca-device and P3HT:PCBM/Ca-device at the applied bias voltage larger than V_{oc} without illumination. For the P3HT/Ca-device, a positively increased MC response is observed at the low magnetic filed (B<~200 mT), which is associated with the dissociation and charge reaction processes of electrical-excited PP pairs from the injected charge carriers (without illumination and the bias voltage large than V_{oc}) as facilitated by the applied electrical and magnetic field. However, the influence from the applied electrical and magnetic field on the total current density of P3HT/Ca-device reaches a saturated level at B>~400 mT. Further increasing the applied magnetic field above ~400 mT did not enlarge the MC response and account for a flat MC curve as shown in Fig. 7.

Blending an electron acceptor, (PCBM), with P3HT as the active layer (a bulk-heterojunction conjugated system) effectively causes the charge separation of the excited states at the donor-acceptor (P3HT-PCBM) interface and therefore markedly changes the MC responses as illustrated in Fig. 7. The MC curve of P3HT:PCBM/Ca-device without illumination is almost inhibited (showing a flat line close to zero) at the low magnetic field from 0 to ~180 mT, but is positively increased with the applied magnetic field at B>~180 mT. The observation of MC curves for the P3HT:PCBM/Ca-device in Fig. 7 confirms very well the results reported by Xu *et al.*, and suggest that such MC responses presented in Fig. 7 are characteristic features for the existence of the intermolecular charge-transfer complexes at the donor-acceptor interface. The dissociation of the intermolecular charge-transfer complexes is interrupted by the strong Coulmbic interactions in donor-acceptor molecules at the low magnetic field.

Therefore, the MC curve is almost zero and has a threshold of increase at B~180 mT. The dissociations of the bound e-h pairs (intermolecular charge-transfer complexes), are facilitated by the high magnetic field (B>~180 mT), which are responsible for the positively increased MC response of P3HT:PCBM/Ca-device.

Figure 8(a) presents the MC curves of P3HT:PCBM/Ca-device with illumination at various bias conditions. Figure 8(b) plots the MC curve of the P3HT:PCBM/Ca-device with illumination versus bias voltage and semi-logarithm *J-V* plot at B=1000mT. The MC curves presented in both Fig.s 8 (a) and (b) have sharply increased (negatively) and inversed MC responses at the bias voltages near the V_{oc}. However, the magnitude of MC responses for P3HT:PCBM/Ca-device is relatively low (<0.1%) as compared to that of P3HT/Ca-device (Fig. 5) at the applied bias lower than the V_{oc} (~0.59V for P3HT:PCBM/Ca-device). This observation can be interpreted in term of quenching most of the photo-excited excitons and PP pairs (magnetic-sensitive) by the separation of oppositely charged carriers at the P3HT-PCBM (donor-acceptor) interface. The dissociation of the charge-transfer complexes at donor-acceptor interface under the influence of the applied magnetic field is also not favorable in this bias regime. Consequently, the P3HT:PCBM/Ca-device has the low MC responses at the bias voltages lower than the V_{oc}. The negative MC responses at $V<V_{oc}$ is due to the reduced charge reaction of unquenched triplet excitons (very little amount in the active layer) under the influence of applied magnetic field. The sharply increased (negatively) MC response at bias voltage of 0.59V in Fig.s 8(a) and (b) is suggested to be due to the drastic reduction of the denominator *I(0)* in Eq. (1), which is nearly zero at the bias voltage close to V_{oc}. The inset of Fig. 8(a) shows the MC curves at the enlarged scale as the biased voltages are nearby V_{oc}. Those curves have a threshold of MC response at the low magnetic field

and are increased negatively or positively at the high magnetic field with the bias voltage larger than V_{oc}, which are associated with the presence of intermolecular charge-transfer complexes in the donor-acceptor interface as discussed in the previous paragraph.

4. Conclusions

In conclusion, the mechanisms to interpret the MC responses for polymer photovoltaic devices made of P3HT and P3HT:PCBM as the active layers are rather complicated. The status of photo- & electrical-excited states (excitons and PP pairs), and intermolecular charge-transfer complexes is susceptible to change by the applied magnetic field and electrical bias. Our results have indicated that positive, negative, and inversion of MC responses can be modulated by the photo illumination, the usage of different metal electrodes, interfacial dipole layer, the applied magnetic and electrical field, and the composition of the polymer active layers. As for P3HT:PCBM-based bulk-heterojunction photovoltaic cells, the charge-transfer complexes would be the critical excited states to influence the overall power conversion efficiency. The magnitude of photocurrent as well as the device performance can be further improved, if the dissociation of the intermolecular charge-transfer complexes is facilitated, probably by manipulating and optimizing the bulk-heterojunction and the polymer/electrode interfaces. The studies to understand the intermolecular charge-transfer complex states in the active layer under the influence of applied magnetic field are currently underway.

Acknowledgments

The author Guo would like to thank the National Science Council (NSC) of Taiwan NSC96-2113-M-006-009-MY3 and the Asian Office of Aerospace Research and

Development (AOARD-08-4076) for financially supporting this research. The author Huang is grateful for the financial support from NSC under grant NSC96-2120-M-006-001.

Reference

1. Braun, D.; Heeger, A. J. *Appl. Phys. Lett*. ***1991***, *58*, 1982
2. Yu, G.; Gao, J.; Hummelen, J. C.; Wudl, F.; Heeger, A. J. *Science* ***1995***, *270*, 1789.
3. Dodabalapur, A.; Katz, H. E.; Torsi, L.; Haddon, R. C. *Science* ***1995***, *269*, 1560.
4. Kalinowski, J. *J. Phys. D: Appl. Phys.* ***1999,*** *32*, R179.
5. Huang, L. S.; Tang, C. W.; Mason, M. G. *Appl. Phys. Lett.* ***1997***, *70*, 152.
6. Günes, S.; Neugebauer, H.; Sariciftci, N. S. *Chem. Rev.* ***2007,*** *107*, 1324.
7. Li, S. H.; Xu, Z.; Ma, L.; Chu, C.W.; Yang, Y. *Appl. Phys. Lett.* ***2007***, *91*, 083507.
8. Sirringhaus, H.; *Adv. Mater.* ***2005***, *17*, 2411.
9. Lee, T. H.; Huang, J. C. A.; Pakhomov, G. L'vovich; Guo, T. F.; Wen, T. C.; Huang, Y. S.; Tsou, C. C.; Chung, C. T.; Lin, Y. C.; Hsu, Y. J. *Adv. Funct. Mater.* ***2008***, *18*, 3036.
10. Mermer, Ö.; Veeraraghavan, G.; Francis, T. L.; Sheng, Y.; Nguyen, D. T.; Wohlgenannt, M.; Köhler, A.; Al-Suti, M. K.; Khan, M. S. *Phys. Rev. B*, ***2005***, *72*, 205202.
11. Desai, P.; Shakya, P.; Kreouzis, T.; Gillin, W. P.; *Phys. Rev. B*, ***2007***, *76*, 235202.
12. Kalinowski, J.; Cocchi, M.; Virgili, D.; Fattori, V.; Di Marco, P. *Phys. Rev. B* ***2004***, *70*, 205303.
13. Desai, P. ; Shakya, P. ; Kreouzis, T. ; Gillin, W. P. ; Morley, N. A. ; Gibbs, M. R. J. *Phys. Rev. B*, ***2007***, *75*, 094423.
14. Wang, F. J.; Ba¨ssler, H.; Vardeny, Z. V. *Phys. Rev. Lett.* ***2008***, 101, 236805.
15. Bergeson, J. D.; Prigodin, V. N.; Lincoln, D. M.; Epstein, A. J.; *Phys. Rev. Lett.* ***2008***, *100,* 067201.

16. Bloom, F. L.; Wagemans, W.; Kemerink, M.; Koopmans, B. *Phys. Rev. Lett.* ***2007***, *99*, 257201.
17. Frankevich, E.; Zakhidov, A.; Yoshino, K.; Maruyama, Y.; Yakushi, K. *Phys. Rev. B*, ***1996***, *53*, 4498.
18. Xu, Z.; Hu, B.; Howe, J. *J. Appl. Phys.* ***2008***, *103*, 043909.
19. Kalinowski, J.; Szmytkowski, J.; Stampor, W. *Chem. Phys. Lett.* ***2003***, *378*, 380.
20. Lee, T. H.; Guo, T. F.; Huang, J. C. A.; Wen, T. C.; *Appl. Phys. Lett.* ***2008***, *92*, 153303.
21. Xiong, Z. H.; Wu, D.; Vardeny, Z. V.; Shi, J. *Nature* ***2004***, *427*, 821
22. Baibich, M. N.; Broto, J. M.; Fert, A.; Van Dau, F. N.; Petroff, F.; Eitenne, P.; Greuzet, G.; Friederich, A.; Chazelas, J. *Phys. Rev. Lett.* ***1988***, *61*, 2472.
23. Binasch, G.; Grünberg, P.; Saurenbach, F.; Zinn, W. *Phys. Rev. B* ***1989***, *39*, 4828.
24. Chiba, D.; Yamanouchi, M.; Matsukura, F.; Ohno, H. *Science* ***2003***, *301*, 943.
25. Desai, P.; Shakya, P.; Kreouzis, T.; Gillin, W. P. *J. Appl. Phys.* ***2007***, 102, 073710.
26. Steiner, U. E.; Ulrich, T. *Chem. Rev.* ***1989***, *89*, 51.
27. Frankevich, E. L.; Lymarev, A. A.; Sokolik, I.; Karasz, F. E.; Blumstengel, S.; Baughman, R. H.; Hörhold, H. H. *Phys. Rev. B*, ***1992***, *46*, 9320.
28. Kalinowski, J.; Cocchi, M.; Virgili, D.; Fattori, V.; Di Marco, P. *Phys. Rev. B*, ***2004***, *70*, 205303.
29. Hu, B.; Wu, Y. N*ature Mater.* ***2007***, *6*, 985.
30. Xu, Z.; Hu, B. *Adv. Funct. Mater.* ***2008***, *18*, 2611
31. Kadashchuk, A.; Vakhnin, A.; Blonski, I.; Beljonne, D.; Shuai, Z.; Brédas, J. L.; Arkhipov, V. I.; Heremans, P.; Emelianova, E.V.; Bässler, H. *Phys. Rev. Lett.* ***2004***, *93*, 066803-1.

32. Scholes, G. D.; Rumbles, G. *Nature Mater.* ***2006****, 5*, 683.

33. Ohkita, H.; Cook, S.; Astuti, Y.; Duffy, W.; Tierney, S.; Zhang, W.; Heeney, M.; McCulloch, I.; Nelson, J.; Bradley, D. D. C.; Durrant, J. R. *J. Am. Chem. Soc.* ***2008***, *130*, 3030.

34. Monkman, A. P.; Burrows, H. D.; Hartwell, L. J.; Horsburgh, L. E.; Hamblett, I.; Navaratnam, S.; *Phys. Rev. Lett.* ***2001***, *86*, 1358.

35. Li, G.; Shrotriya, V.; Huang, J.; Yao, Y.; Moriarty, T.; Emery, K.; Yang, Y. *Nature Mater.* ***2005***, *4*, 864.

36. Guo, T. F.; Wen, T. C.; Pakhomov, G. L.; Chin, X.G.; Liou, S. H.; Yeh, P. H.; Yang, C. H. *Thin Solid Film* ***2008***, *516*, 3138.

37. Mihailetchi, V. D.; Blom, P. W. M.; Hummelen, J. C.; Rispens. M. T.; *J. Appl. Phys.* ***2003***, *94*, 6849

38. Brabec, C. J.; Cravino, A.; Meissner, D.; Sariciftci, N. S.; Fromherz, T.; Rispens, M. T.; Sanchez, L.; Hummelen, J. C. *Adv. Funct. Mater.* ***2001***, *11*, 374.

Figure captions

FIG. 1. (a) The formation of intra- and inter-molecular excited PP pairs from excitons. (b) The singlet and triplet electronic configurations of excitons and PP pairs.

FIG. 2. A schematic drawing that illustrates the device configuration and the measurement of MC responses for the polymer diodes under the applied magnetic field with illumination.

FIG. 3. MC curves of the I_{sc} for P3HT/Al-device (○) and P3HT/Ca-device (□) with illumination.

FIG. 4. MC curves of the I_{sc} for P3HT/LiF(X nm)/Ca-device at B=1000mT of X= 0 (□),1.5 (△), and 5.0 (■). The inset presents the thickness of LiF layer versus MC response (○) at B=1000mT and abs. I_{sc} plots (●).

FIG. 5. (a) MC curves of P3HT/Ca-device with the illumination in the bias voltages of 0V (○), 0.50V (□), 0.90V (◇), 1.00V (△), 1.10V (▽), and 1.50V (●), (b). MC curve (□) of the P3HT/Ca-device with illumination versus bias voltage and semi-logarithm current-voltage (*J*-*V*) plot (○) at B=1000mT.

FIG. 6. The energy diagrams of P3HT/Ca-device and the flow directions of I_d and I_p at the applied voltages (a) below and (b) above the V_{oc}.

FIG. 7. MC curves of P3HT/Ca-device (○) and P3HT:PCBM/Ca-device (□) at the

applied bias voltage larger than V_{oc} without illumination.

FIG. 8. (a) MC curves of P3HT:PCBM/Ca-device with the illumination in bias voltages of 0.50V (◯), 0.56V (□), 0.58V (◇), 0.59V(■), 0.60V (△), 0.62V (▽) and 0.64V (●). The inset shows the MC curves at the enlarged scale in the biased voltages of 0.50V (◯), 0.56V (□), 0.58V (◇), 0.62V (▽) and 0.64V (●). (b) MC curve (□) of the P3HT:PCBM/Ca-device with illumination versus bias voltage and semi-logarithm current-voltage (*J*-*V*) plot (◯) at B=1000mT.

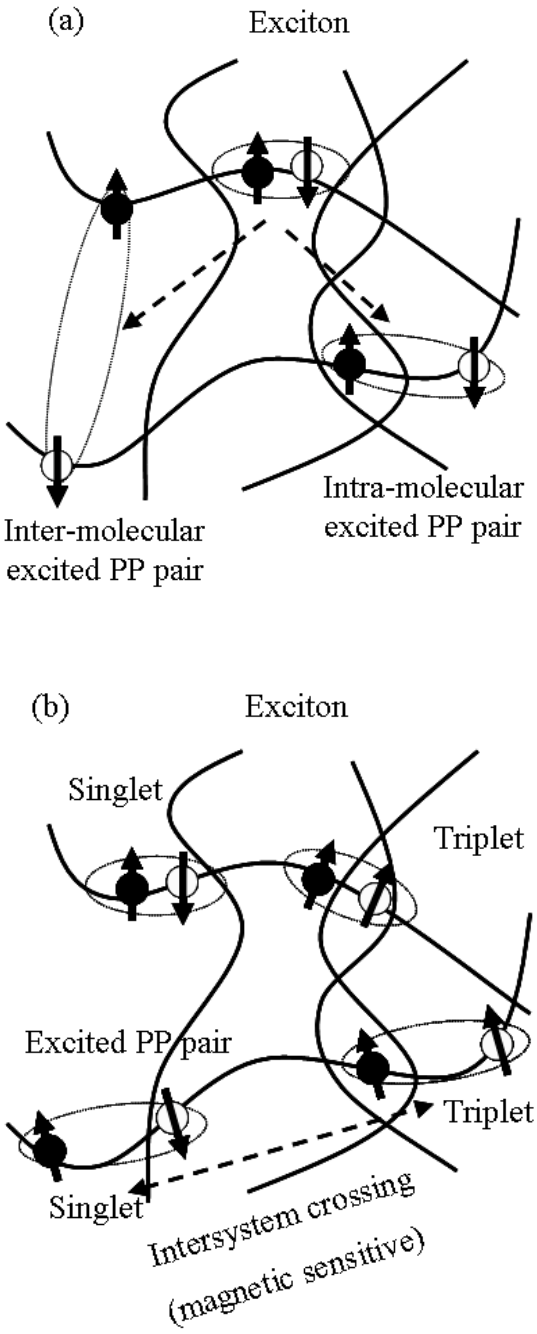

Figure 1, Lee *et al.*

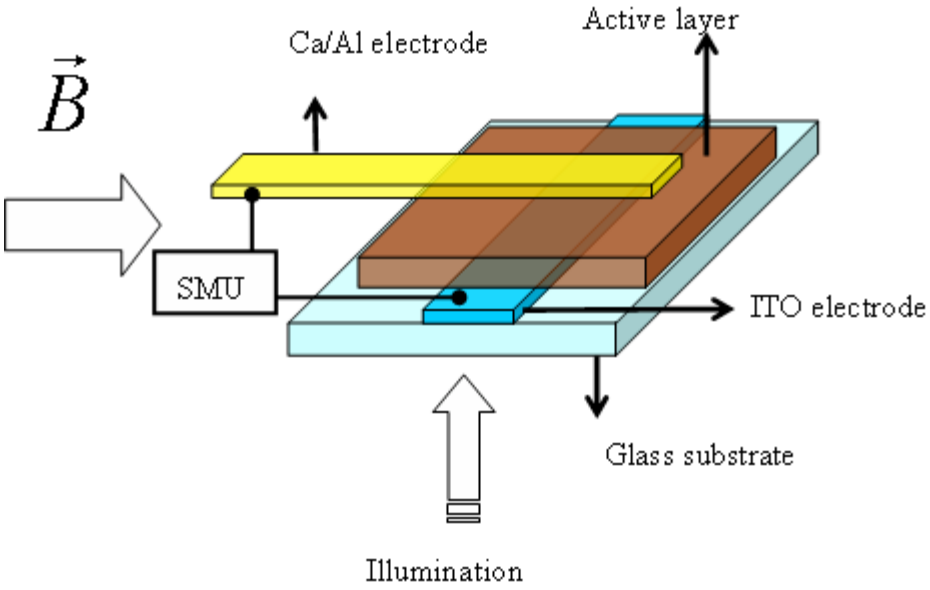

Figure 2, Lee *et al.*

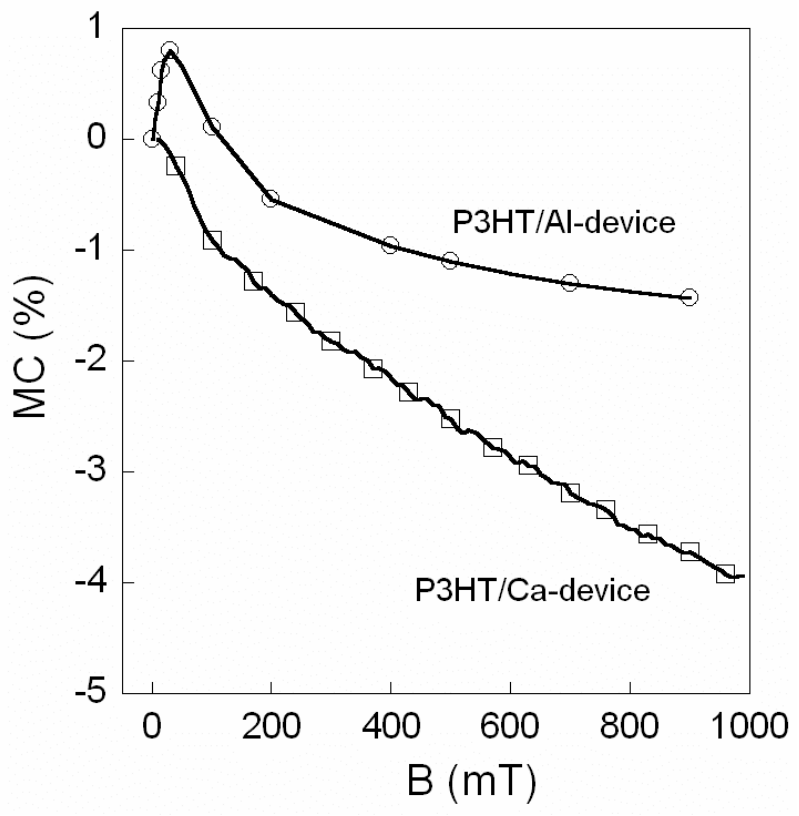

Figure 3, Lee *et al.*

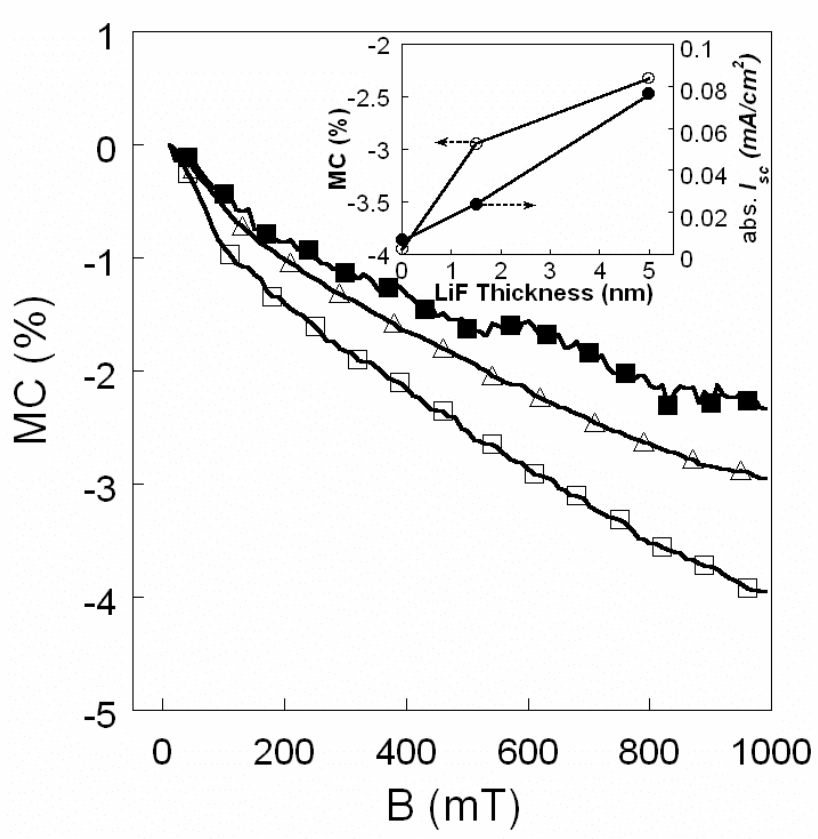

Figure 4, Lee *et al.*

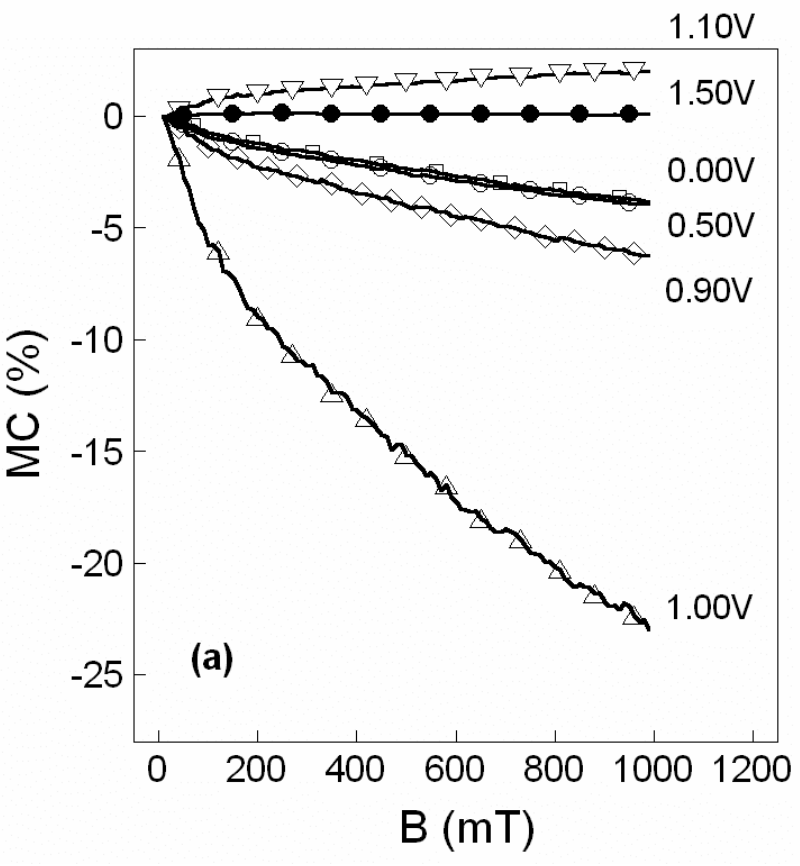

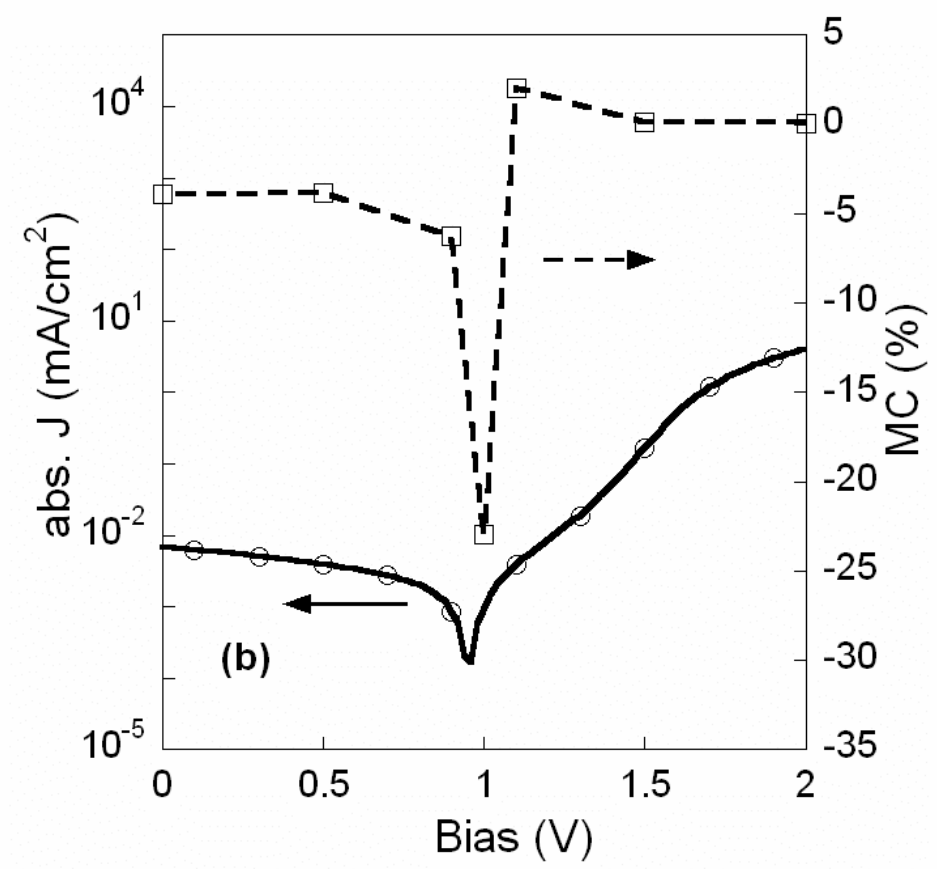

Figure 5, Lee *et al.*

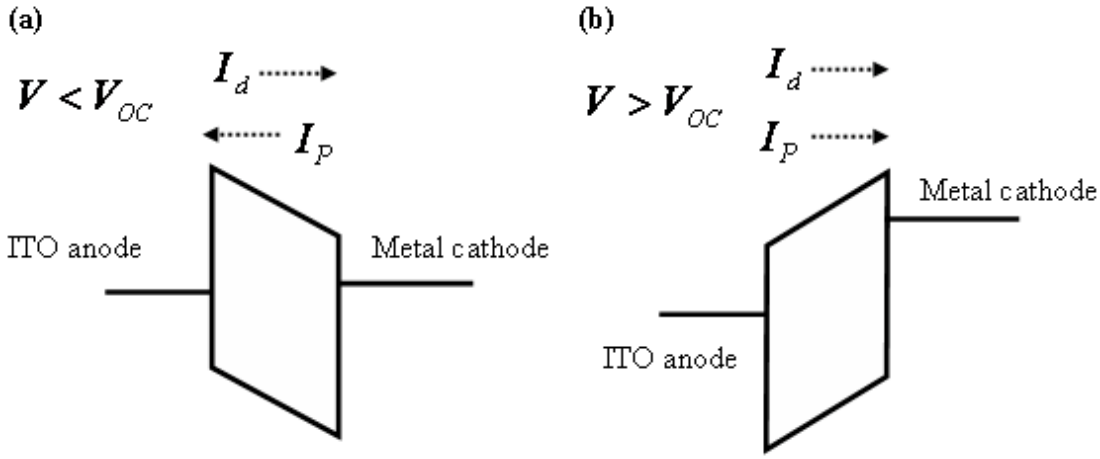

Figure 6, Lee *et al.*

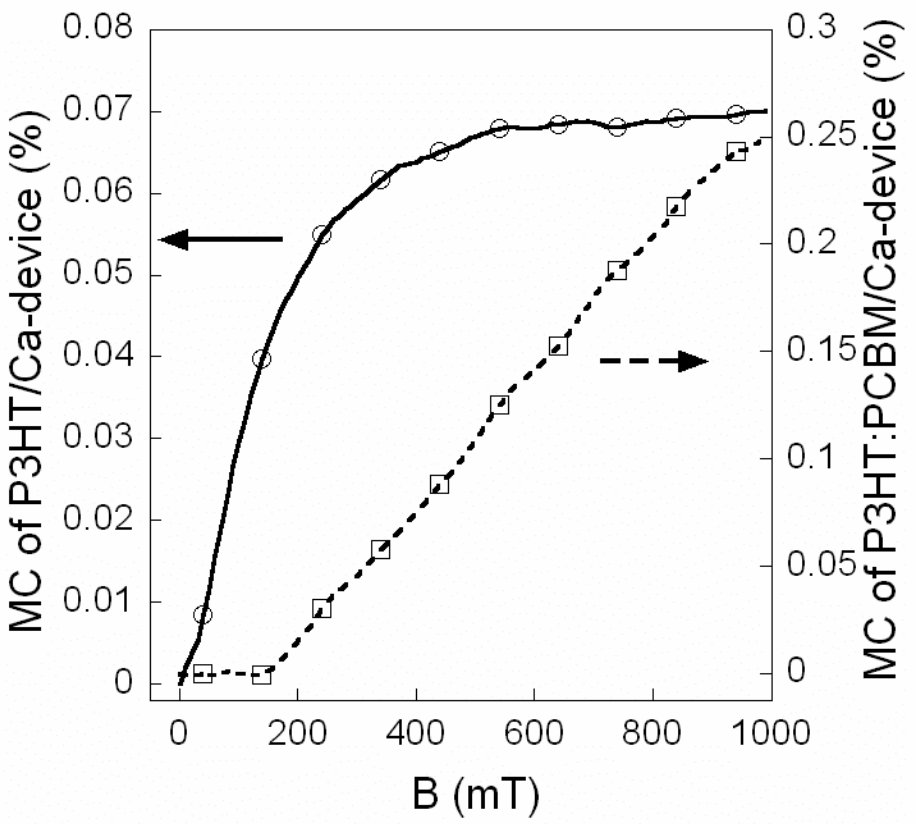

Figure 7, Lee *et al.*

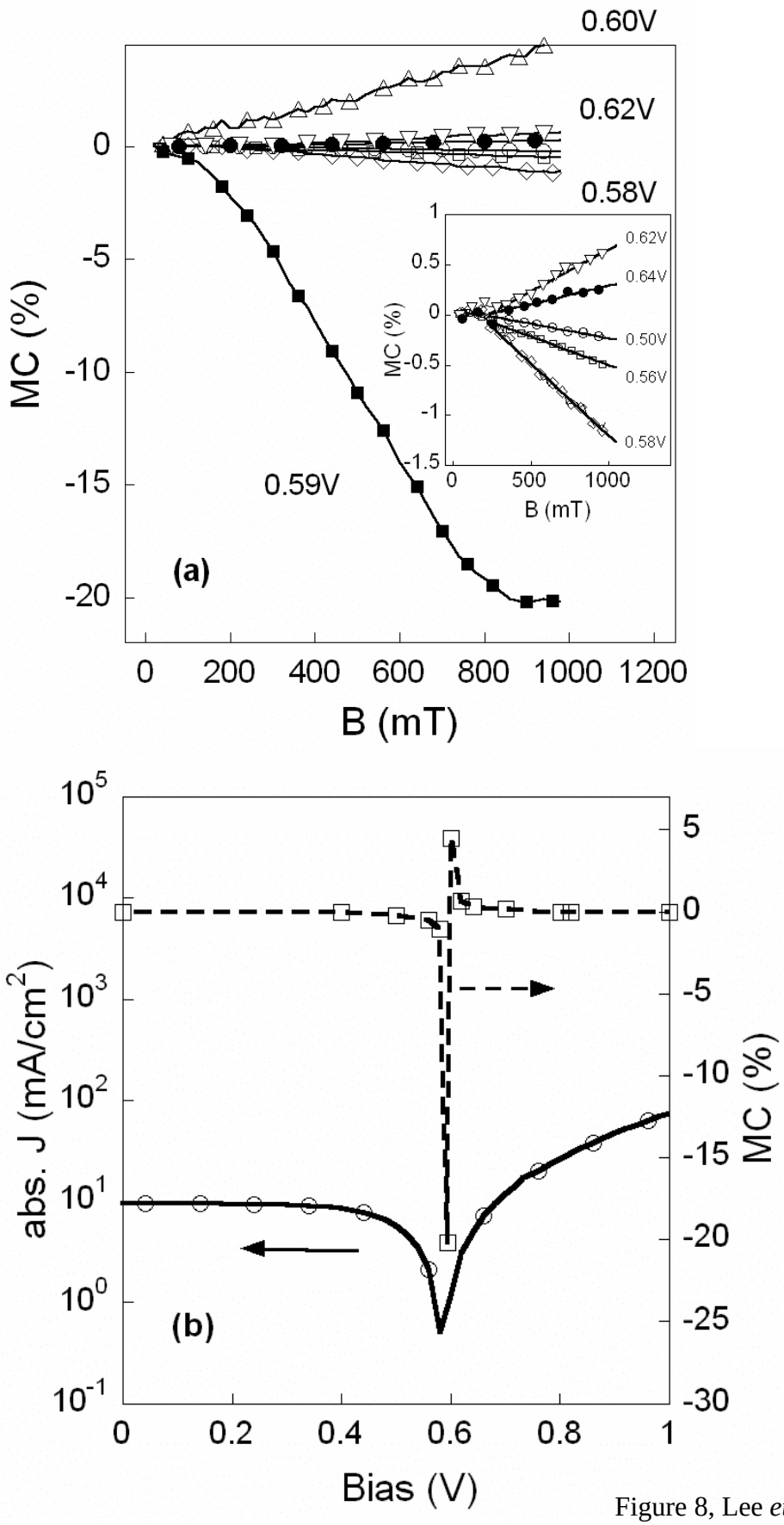

Figure 8, Lee *et al.*